CHAPTER 3

RESULTS AND DISCUSSION

In this Chapter, the particles properties of unloaded WO_3 and Pt-loaded WO_3 synthesized by FSP and the hydrothermal method are discussed by XRD, BET, SEM with EDS –dot mapping mode, HRTEM. Gas sensing films of all samples were tested towards flammable gases (H_2, C_2H_5OH , C_2H_4 and CO), environmentally hazardous gas (NO_2).

3.1 Particles properties

3.1.1 X–ray diffraction analysis (XRD)

Figure 3.1(a) shows the XRD patterns of unloaded WO_3, 0.25–1.0 wt.% Pt-loaded WO_3 nanoparticles (P0-P1), Au/Al_2O_3 substrate (Au/Al_2O_3 substrate) and corresponding WO_3 sensing films after annealing (S0-S1). It can be clearly seen that P0-P1 samples were crystalline and all peaks can be well matched to JCPDS file No.83−0950, which corresponds to WO_3 monoclinic structure. However, diffraction peaks of Pt were not found in these patterns. This absence should be due to the fact that concentrations of Pt were very low and XRD does not have sufficient sensitivity to detect it. XRD peaks of sensing films (S0-S1) confirm the presence of monoclinic WO_3 structure of the films. In addition, it is seen that S0-S1 have different XRD peak intensities compared to their corresponding nanoparticles (P0-P1), indicating changes in texturization of the crystal plane orientation after sensing films preparation.

Figure 3.1 (b) shows the XRD patterns of unloaded WO_3 and 0.25–1.0 wt.% Pt-loaded WO_3 nanoparticles (H0-H1). It can be seen that all samples were highly crystalline, and all peaks can match to the monoclinic structure of WO_3 (JCPDS No. 04–006–7123). However, Pt peaks were not found in these patterns. It can be assumed that the size of Pt particles were very small, which were later proved by the HRTEM results.

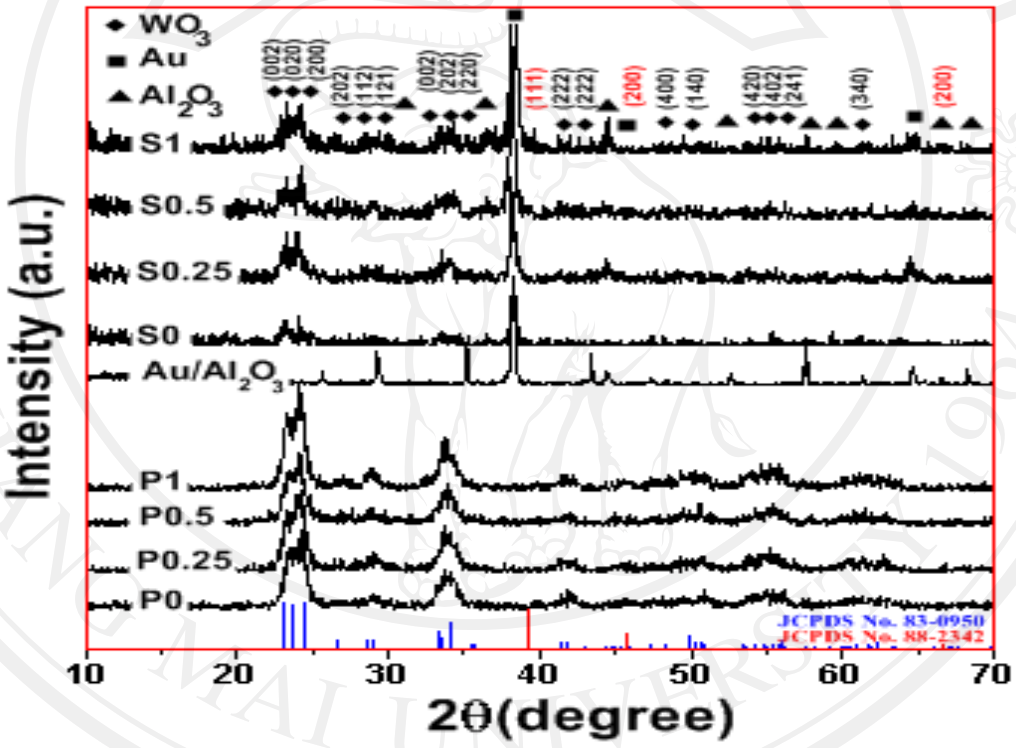

Figure 3.1(a) XRD patterns of flame-spray-made (5/5) unloaded WO_3 as-prepared (P0), 0.25–1.0 wt.% Pt-loaded WO_3 (P0.25-P1), Au/Al_2O_3 substrate (Au/Al_2O_3), and samples P0, P0.25, P0.5, and P1 were spin-coated on Au/Al_2O_3 substrate after annealing and sensing test (S0, S0.25, S0.5, and S1) ((◆) WO_3; (▲) Al_2O_3; (■) Au).

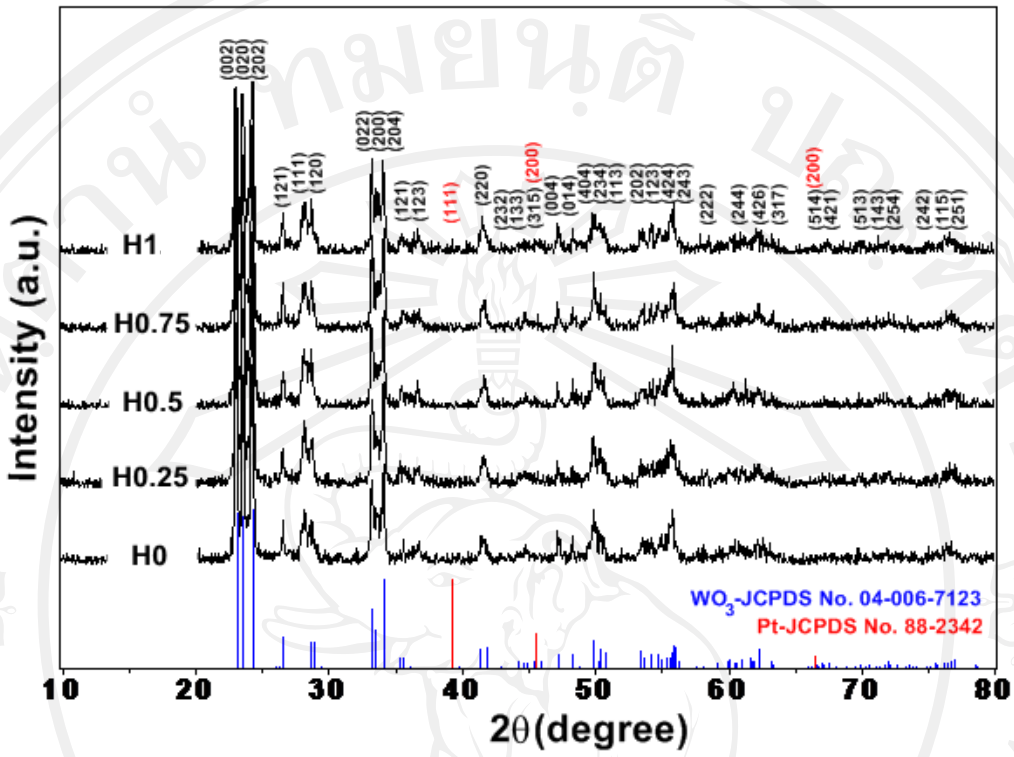

Figure 3.1(b) XRD patterns of WO_3 loaded with different contents of Pt. From H0-H1, the doping ration of Pt/W was 0, 0.25, 0.5, 0.75 and 1.0 wt.%, respectively.

3.1.2 BET analysis

The average BET equivalent particle diameters (d_{BET}) as shown in Table 3.1 were calculated using the density of WO_3 and Pt to take into account for their weight contents in different loading. It can be seen that SSA_{BET} increases while d_{BET} decreases with Pt concentration. The results can be explained that d_{BET} of Pt-loaded WO_3 nanoparticles would be the ordinary average size of the combined Pt and WO_3 nanoparticles. With increasing Pt loading, the number of Pt particles increased and hence the average particles would decrease because the size of Pt nanoparticles was expected to be much smaller than those of WO_3 nanoparticles.

Table 3.1 shows SSA_{BET} and d_{BET} comparison of unloaded WO_3 and 0.25–1.0 wt.% Pt-loaded WO_3 nanoparticles synthesized by FSP and the hydrothermal method.

Table 3.1 SSA_{BET} and d_{BET} of unloaded WO_3 and 0.25–1.0 wt.% Pt-loaded WO_3 nanoparticles synthesized by FSP and the hydrothermal method.

SAMPLE	SPECIFIC SURFACE AREA SSA_{BET} (m^2/g)	PARICLE DIAMETER d_{BET} (nm)
P0	84.12	9.96
P0.25	96.57	8.70
P0.5	94.92	8.87
P0.75	97.11	8.69
P1	96.19	8.80
H0	9.94	84.30
H0.25	12.39	67.80
H0.5	12.66	66.52
H0.75	15.07	56.03
H1	15.04	56.28

3.1.3 Scanning electron microscopy (SEM)

Figure 3.2 shows the morphology of highly crystalline flame–made (5/5) (a) unloaded WO_3 (P0) and (b-e) 0.25–1.0 wt.% Pt-loaded WO_3 nanoparticles (P0.25-P1) for SEM analysis. It can be seen that nanoparticles were spherical in shape, and well dispersed without evidence of aggregation. The average particle size ranges from 10 to 20 nm. From this observation, it was found that the rough morphology and the rough particle sizes were not changed with increasing Pt loading levels. Nevertheless, the accurate sizes and morphology of the nanoparticles can be estimated from the HRTEM analysis. While the SEM images provide 3–D morphology and can estimate particle sizes, TEM images reveal more internal structure and a more accurate measurement of particle size and morphology than SEM.

SEM images of (a) unloaded WO_3 (H0) and (b-e) 0.25–1.0 wt.% Pt-loaded WO_3 nanoparticles (H0.25-H1) shown in Figure 3.3 revealed platelet structure regardless of the different Pt concentration employed. The powders were seen as loose agglomerations with a plate size ranging from roughly 40 to 500 nm wide and 20–40 nm thick. Note that finer, individual platelets were not clearly observed by SEM study due to its limited resolution.

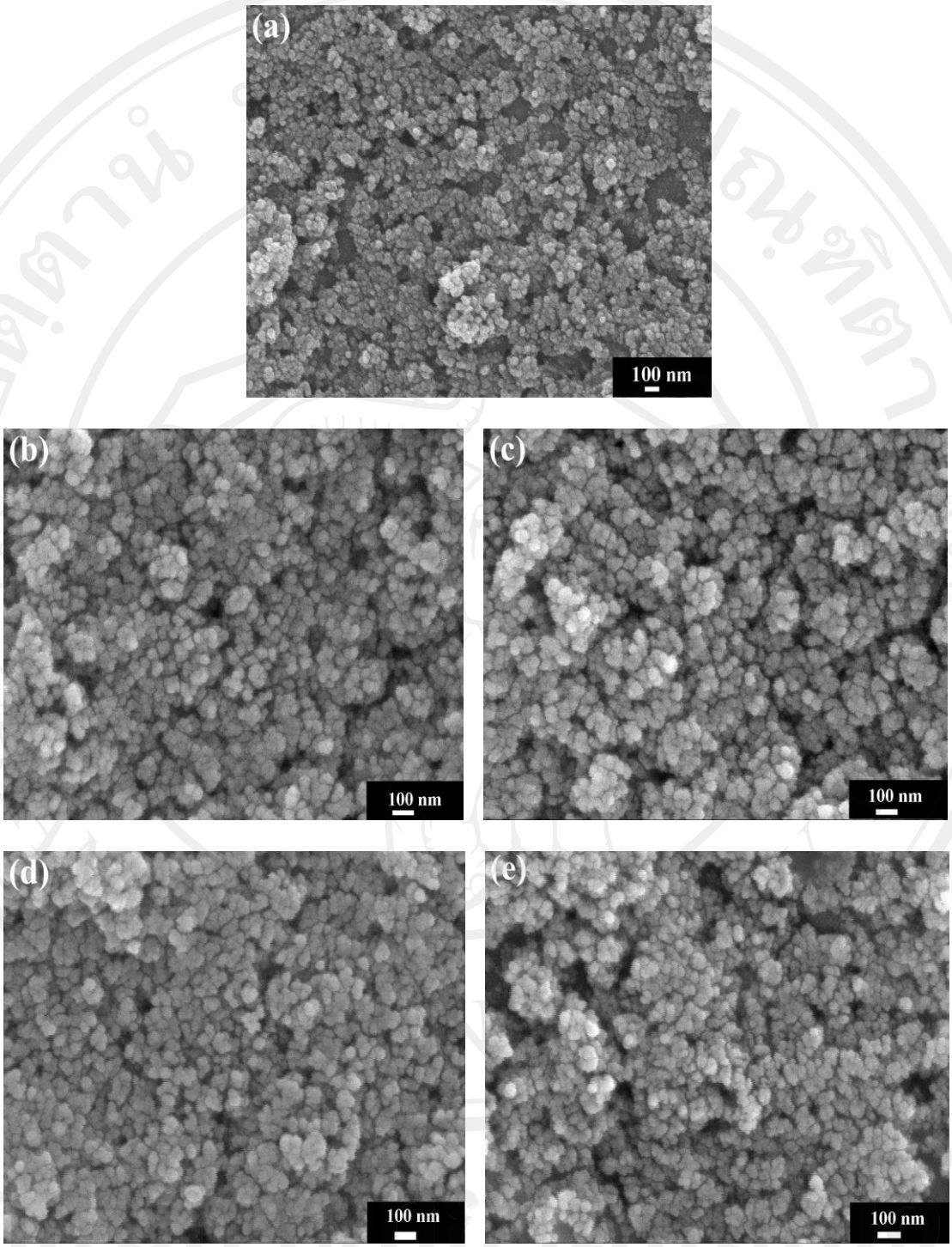

Figure 3.2 The morphology of highly crystalline flame–made (5/5) (a) unloaded WO_3 (P0) (b) 0.25 wt.% Pt-loaded WO_3 (P0.25) (c) 0.5 wt.% Pt-loaded WO_3 (P0.5) (d) 0.75 wt.% Pt-loaded WO_3 (P0.75) and (e) 1.0 wt.% Pt-loaded WO_3 (P1) nanoparticles for SEM analysis.

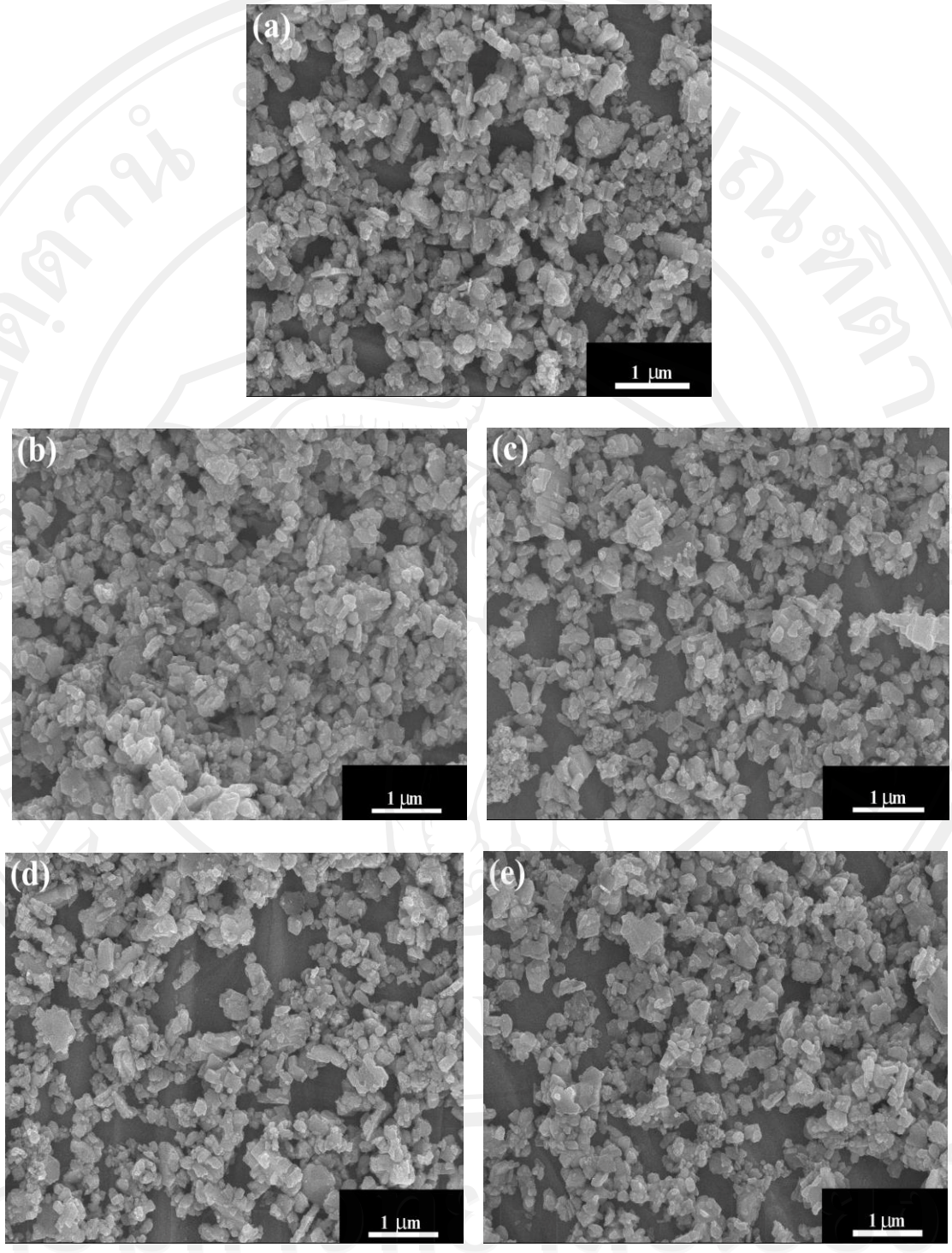

Figure 3.3 The morphology of (a) unloaded WO_3 (H0) (b) 0.25 wt.% Pt-loaded WO_3 (H0.25) (c) 0.5 wt.% Pt-loaded WO_3 (H0.5) (d) 0.75 wt.% Pt-loaded WO_3 (H0.75) and (e) 1.0 wt.% Pt-loaded WO_3 (H1) nanoparticles for SEM analysis.

Figures 3.4 and 3.5 show EDS spectrum and EDS–dot mapping images of all elements in (a) unloaded WO_3 (P0) (b) 1.0 wt.% Pt-loaded WO_3 (P1) (c) unloaded WO_3 (H0) and (d) 1.0 wt.% Pt-loaded WO_3 (H1) nanoparticles. It can be seen that W, O and Pt elements were quite evenly distributed over the area. In addition, the density of Pt sites was approximately a few percents of those of W and O sites. This was consistent with expected elemental composition. The average Pt concentrations of P1 and H1 nanoparticles were estimated by EDS quantitative analysis software (Oxford Instrument) to be 1.33% and 1.21%, which is in good agreement with the intended concentration. However, the concentrated amount of element compositions was slightly changed depending on the different selected area in EDS analysis. Nevertheless, the EDS spectrum and mapping confirm the existence of Pt and indicates that Pt is uniformly dispersed in the mixture of nanoparticles.

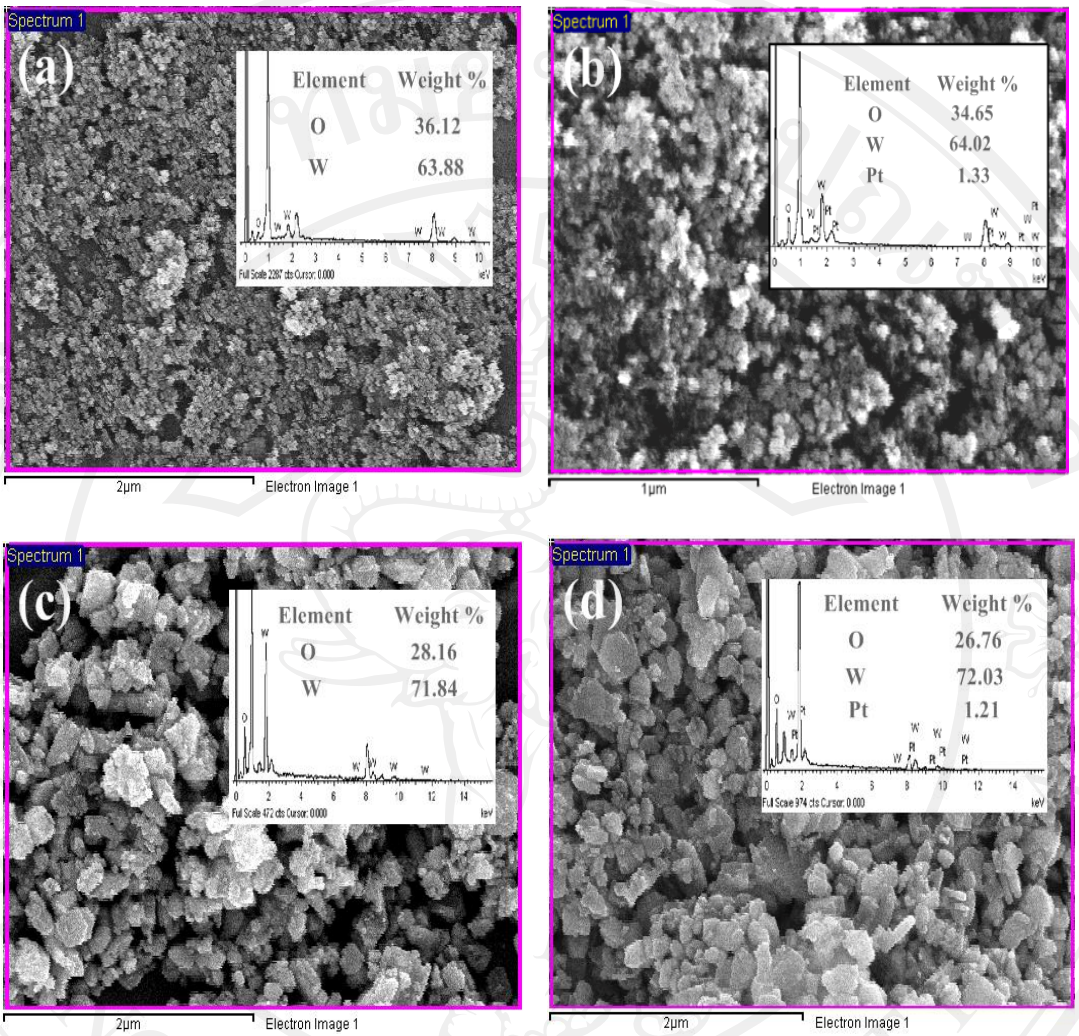

Figure 3.4 The EDS spectra images of all elements in the (a) unloaded WO_3 (P0) (b) 1.0 wt.% Pt-loaded WO_3 (P1) (c) unloaded WO_3 (H0) and (d) 1.0 wt.% Pt-loaded WO_3 (H1) nanoparticles.

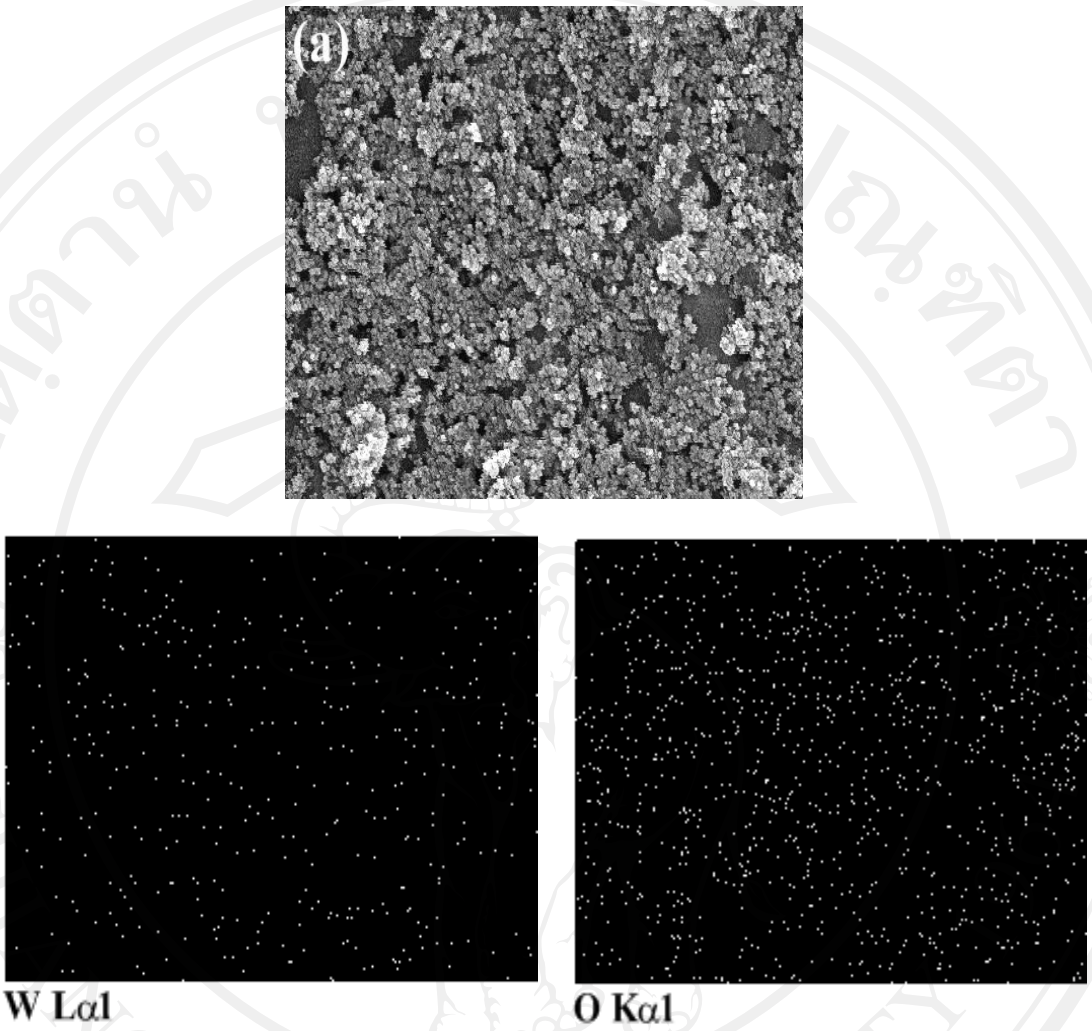

Figure 3.5 (a) EDS–dot mapping images of all elements in the unloaded WO_3 (P0) nanoparticles.

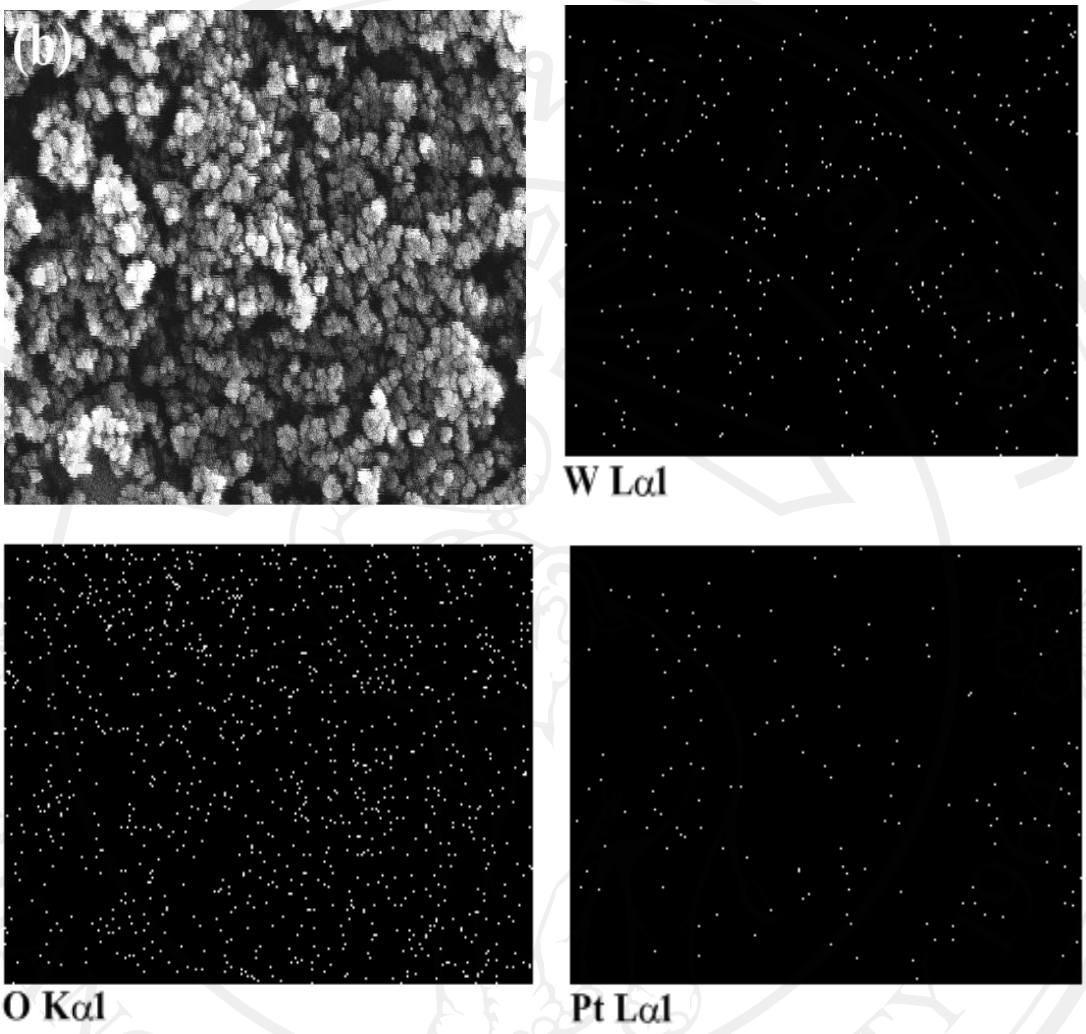

Figure 3.5 (b) EDS–dot mapping images of all elements in the 1.0 wt.% Pt-loaded WO_3 (P1) nanoparticles.

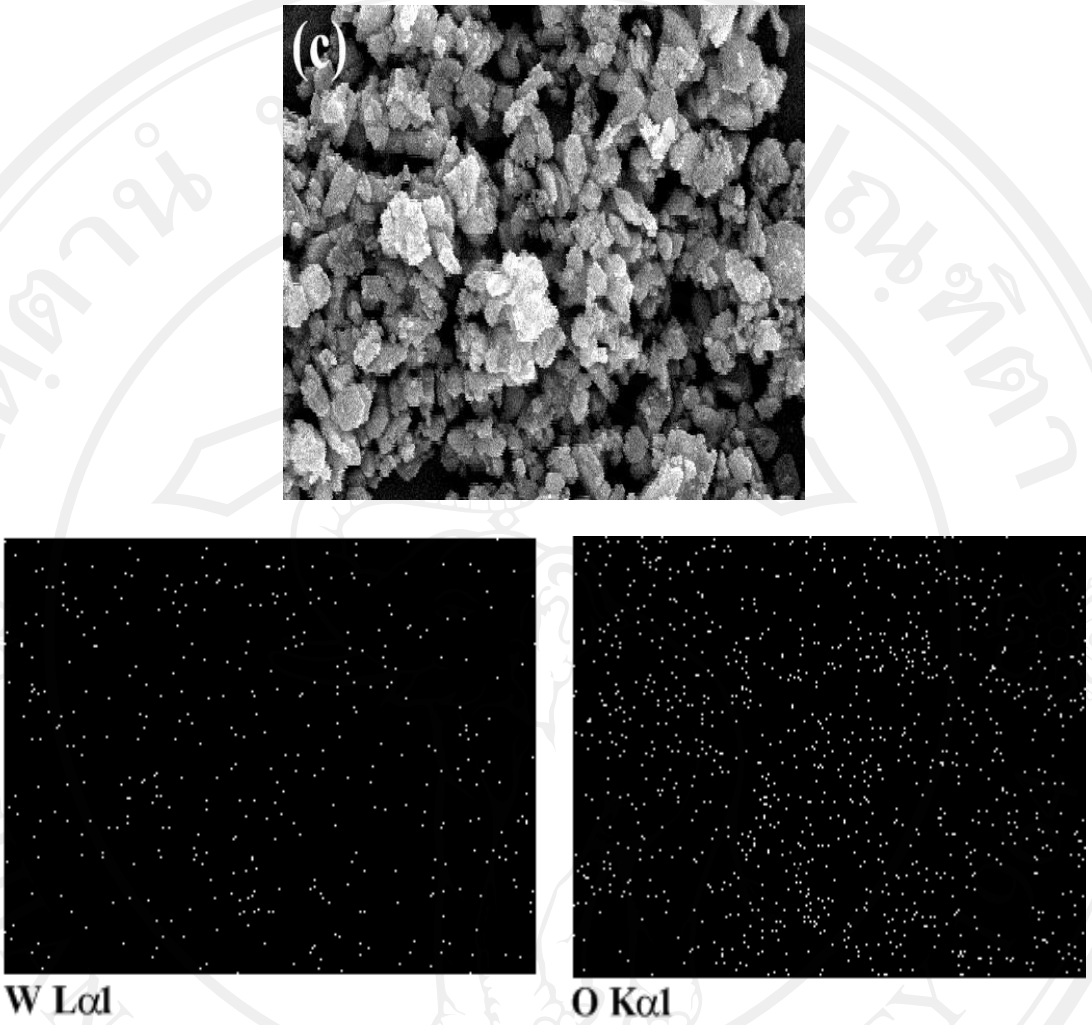

Figure 3.5 (c) EDS–dot mapping images of all elements in the unloaded WO_3 (H0) nanoparticles.

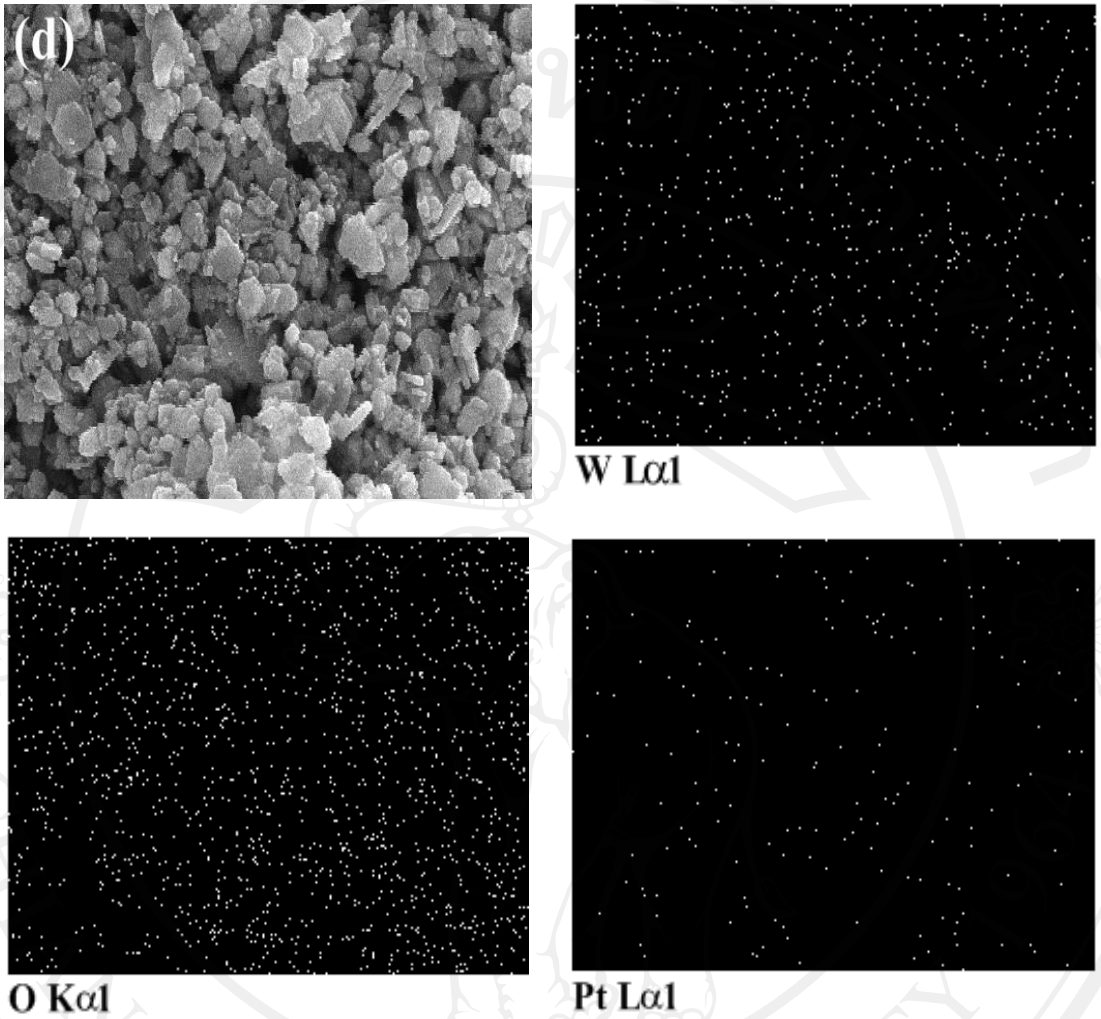

Figure 3.5 (d) EDS–dot mapping images of all elements in the 1.0 wt.% Pt-loaded WO_3 (H1) nanoparticles.

3.1.4 High resolution transmission electron microscopy (HRTEM)

Figure 3.6 shows HRTEM images of (a) unloaded WO_3 (P0) (b) 1.0 wt.% Pt-loaded WO_3 (P1) (c) unloaded WO_3 (H0) and (d) 1.0 wt.% Pt-loaded WO_3 (H1) nanoparticles. The unloaded WO_3 nanoparticles (Figure 3.6(a)) and 1.0 wt.% Pt-loaded WO_3 (Figure 3.6(b)) were seen as particles having a clear spherical morphology. The particles sizes were found to be almost in the same range of ~10 nm for both cases, which was in good agreement with the BET data. The crystallite sizes of spherical unloaded WO_3 (P0) and 1.0 wt.% Pt-loaded WO_3 (P1) were found to be ranging from 5−20 nm. For unloaded WO_3 (H0) and 1.0 wt.% Pt-loaded WO_3 (H1) nanoparticles (Figures 3.6(c) and (d)), it was observed that platelet particle having the average size of 80±10 nm long and 50±5 nm thick. HRTEM images show that very small Pt nanoparticles as uniformly dispersed on the surface of larger WO_3 particles. The size of Pt nanoparticles is small than 1 nm for 1.0 wt.% Pt-loaded WO_3. The uniform Pt dispersion throughout WO_3 support is very important for enhancing the gas sensing properties of metal oxide [88, 146].

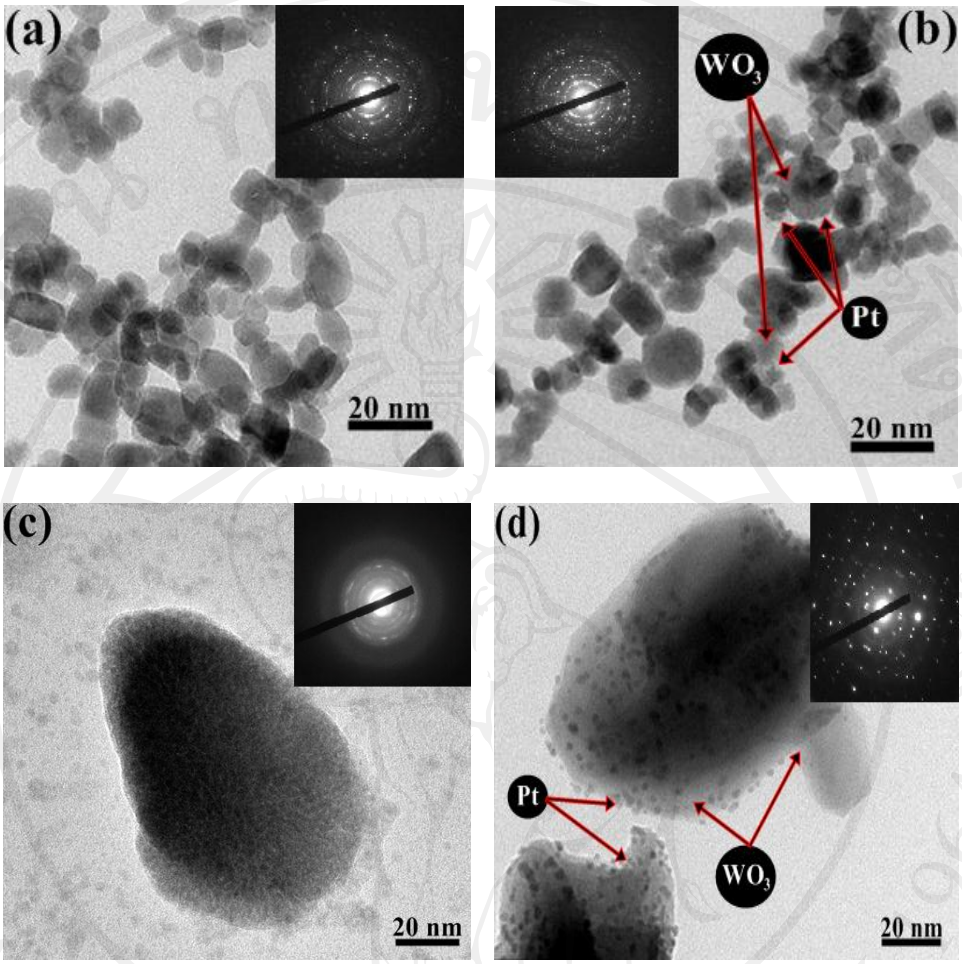

Figure 3.6 HRTEM images of (a) unloaded WO_3 (P0) (b) 1.0 wt.% Pt-loaded WO_3 (P1) (c) unloaded WO_3 (H0) and (d) 1.0 wt.% Pt-loaded WO_3 (H1) nanoparticles.

3.1.5 SEM sensing layer

The cross-section, film thickness and surface morphology of the sensing film layer (S0) after annealing and gas sensing are further characterized using SEM analysis as shown in Figures 3.7 (a) and (b). It can be seen that the films were nanoporous with very fine grain nanoparticle structures. The film thickness of sensing film was estimated to be approximately (a) 30 μm and (b) 1 μm, which could provide

tremendously benefit gas sensing because the films were nanoporous and hence its specific surface area for gas sensing is increased with the film thickness.

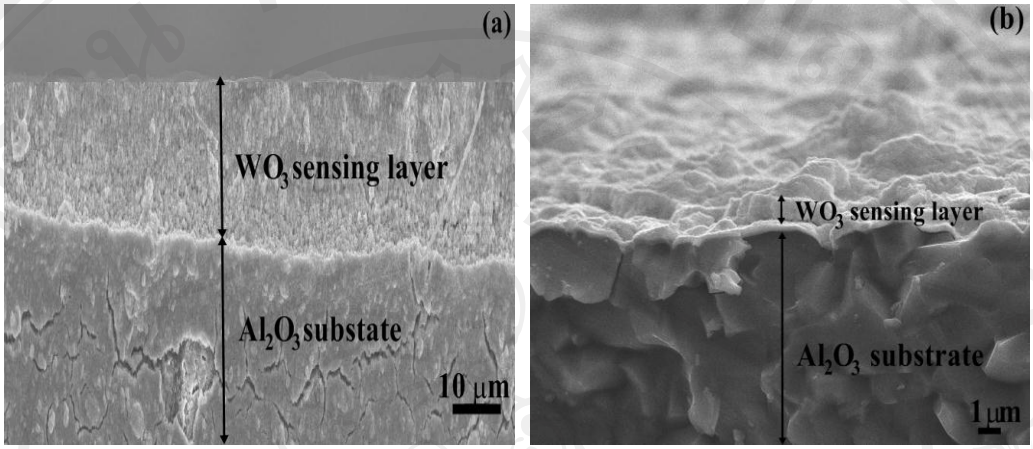

Figure 3.7 (a) SEM micrographs of sensor (S0) based on unloaded WO_3 (P0) and (b) sensor (S0) based on unloaded WO_3 (H0) nanoparticles.

Figures 3.8 (a-d) show EDS line scan images of all elements in the unloaded WO_3 and 1.0 wt.% Pt-loaded WO_3 sensors. It can be seen that W, O and Pt elements were quite evenly distributed over the entire area. In addition, the density of Pt sites was approximately a few percents of those of W and O sites. This was consistent with expected elemental composition. The EDS line confirms the existence of Pt and indicates that Pt was uniformly dispersed on the surface of nanoparticles.

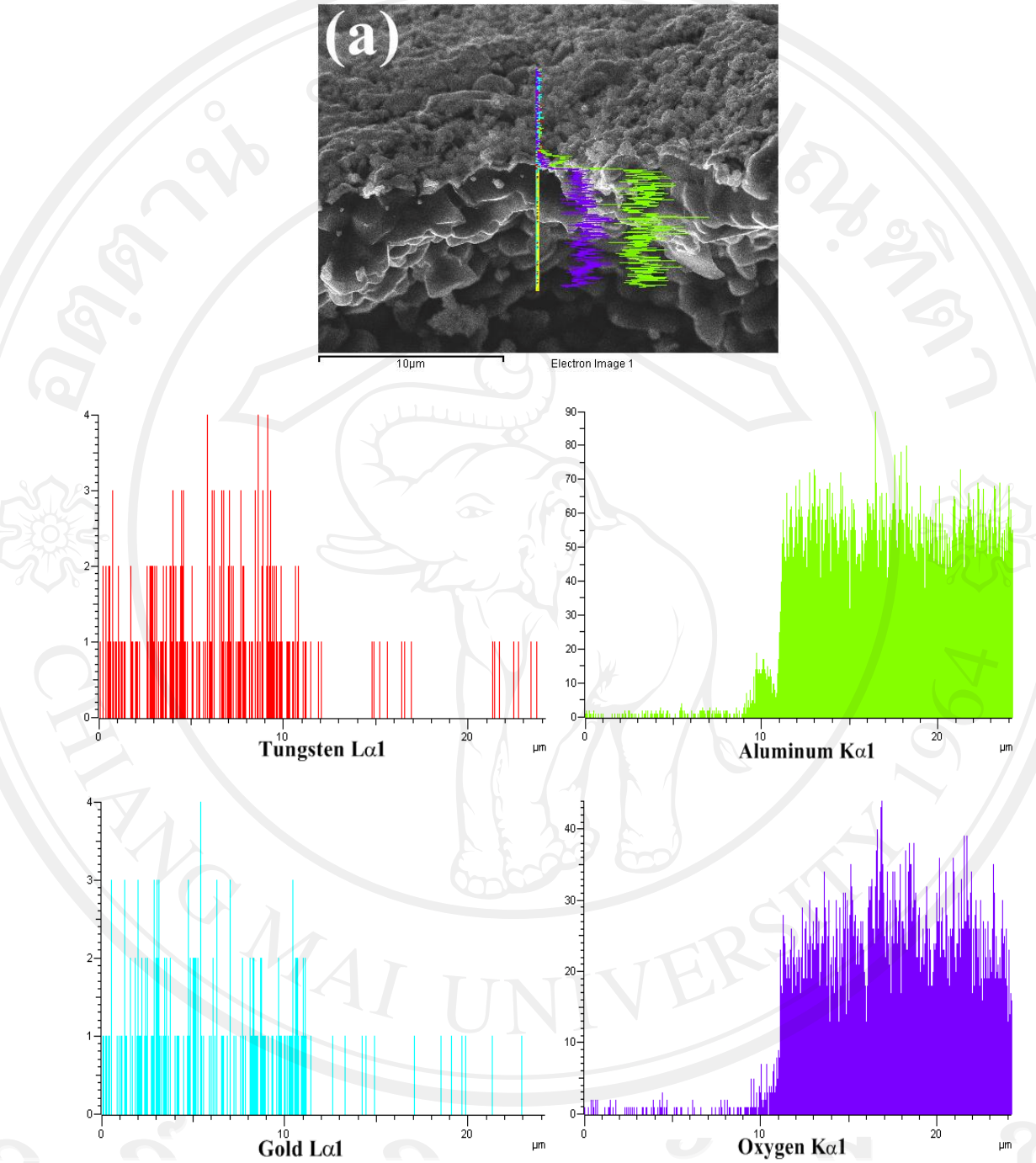

Figure 3.8 (a) The EDS line scan mode–SEM analysis of sensor (S0) based on unloaded WO_3 nanoparticles (P0). The histograms showed the elemental compositions of samples. The lines scans correspond to W, Al, Au, and O elements.

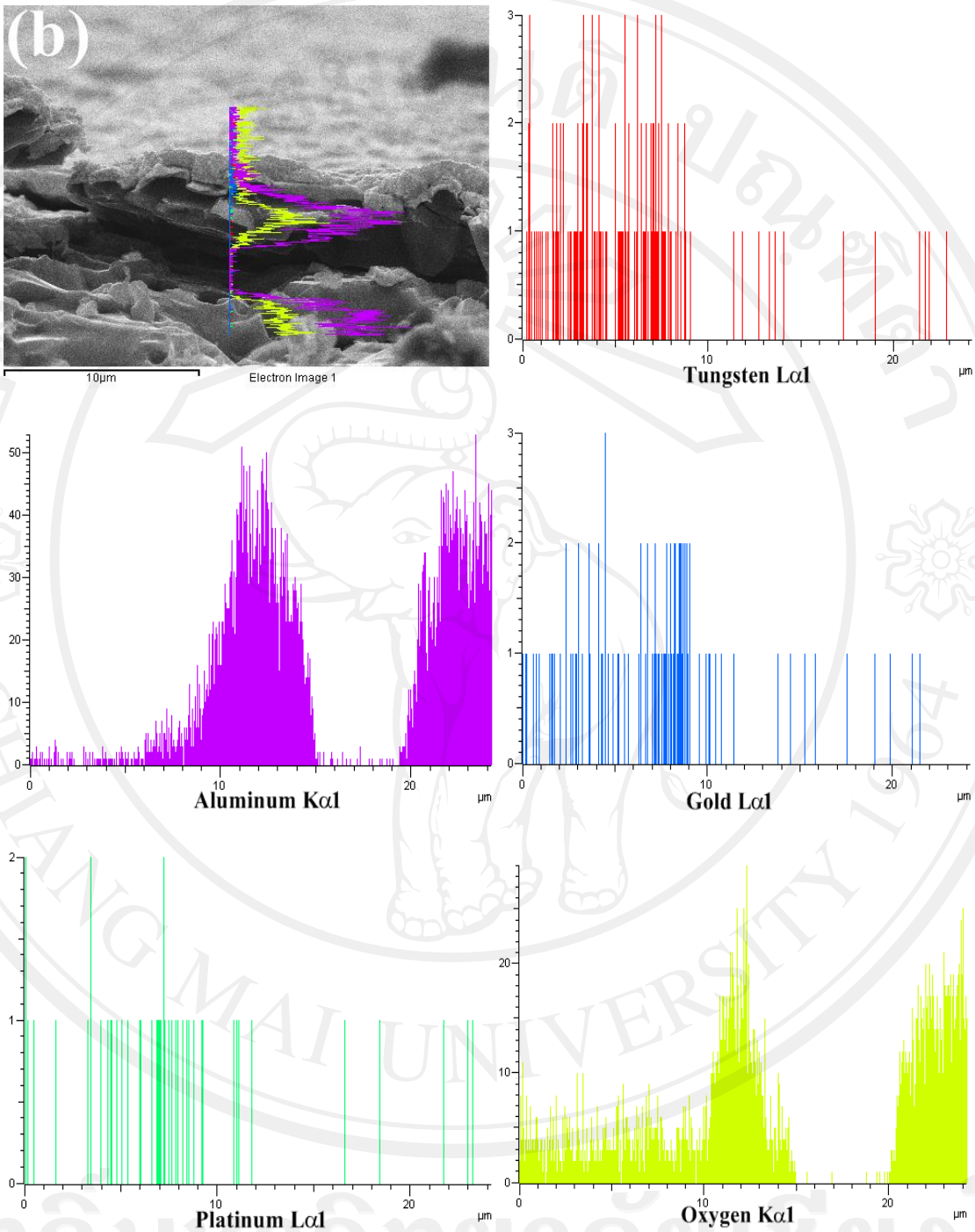

Figure 3.8 (b) The EDS line scan mode–SEM analysis of sensor (S1) based on 1.0 wt.% Pt-loaded WO_3 nanoparticles (P1). The histograms showed the elemental compositions of samples. The lines scans correspond to W, Al, Au, Pt and W elements.

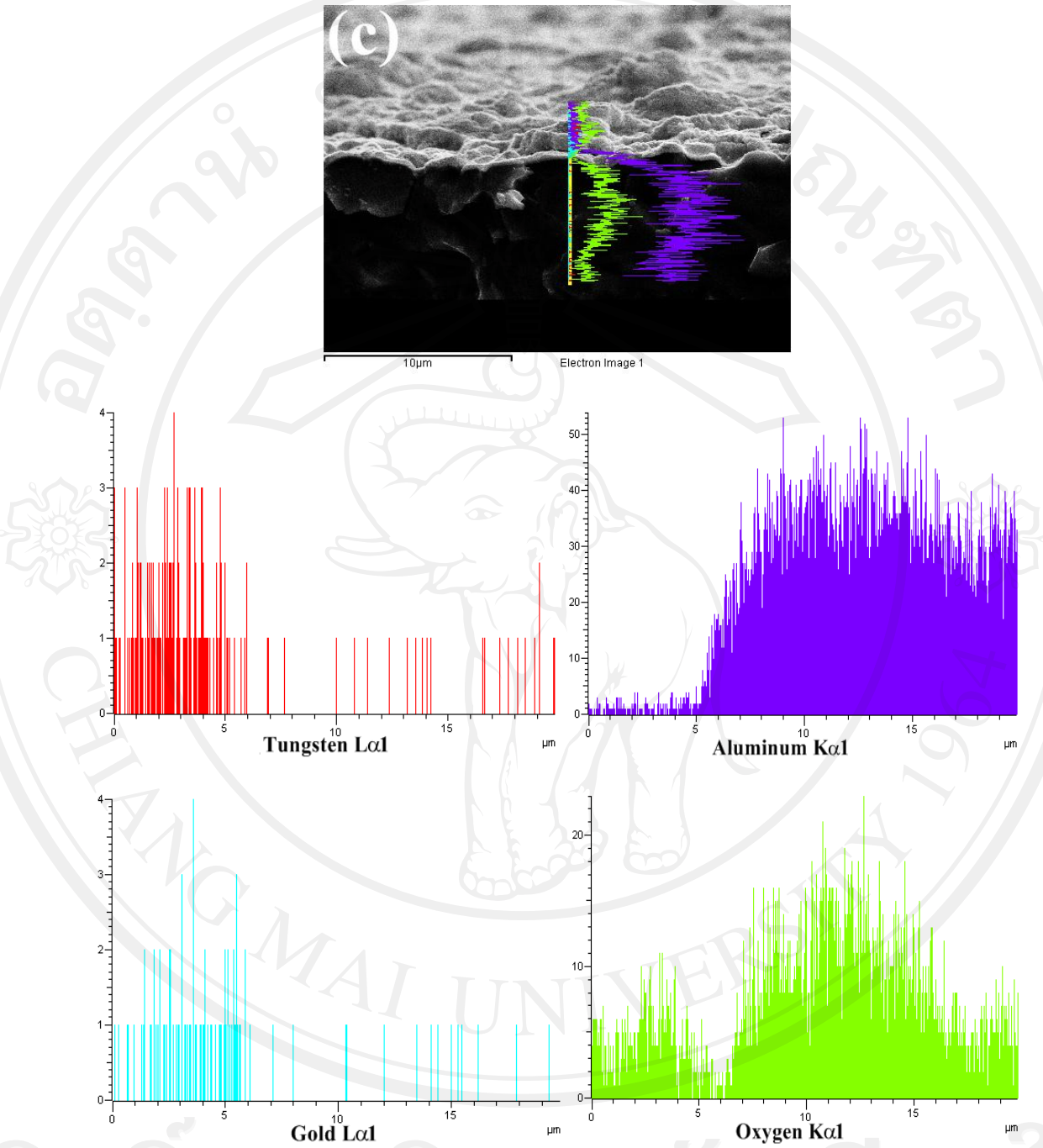

Figure 3.8 (c) The EDS line scan mode–SEM analysis of sensor (S0) based on unloaded WO_3 nanoparticles (H0). The histograms showed the elemental compositions of samples. The lines scans correspond to W, Al, Au, and O elements.

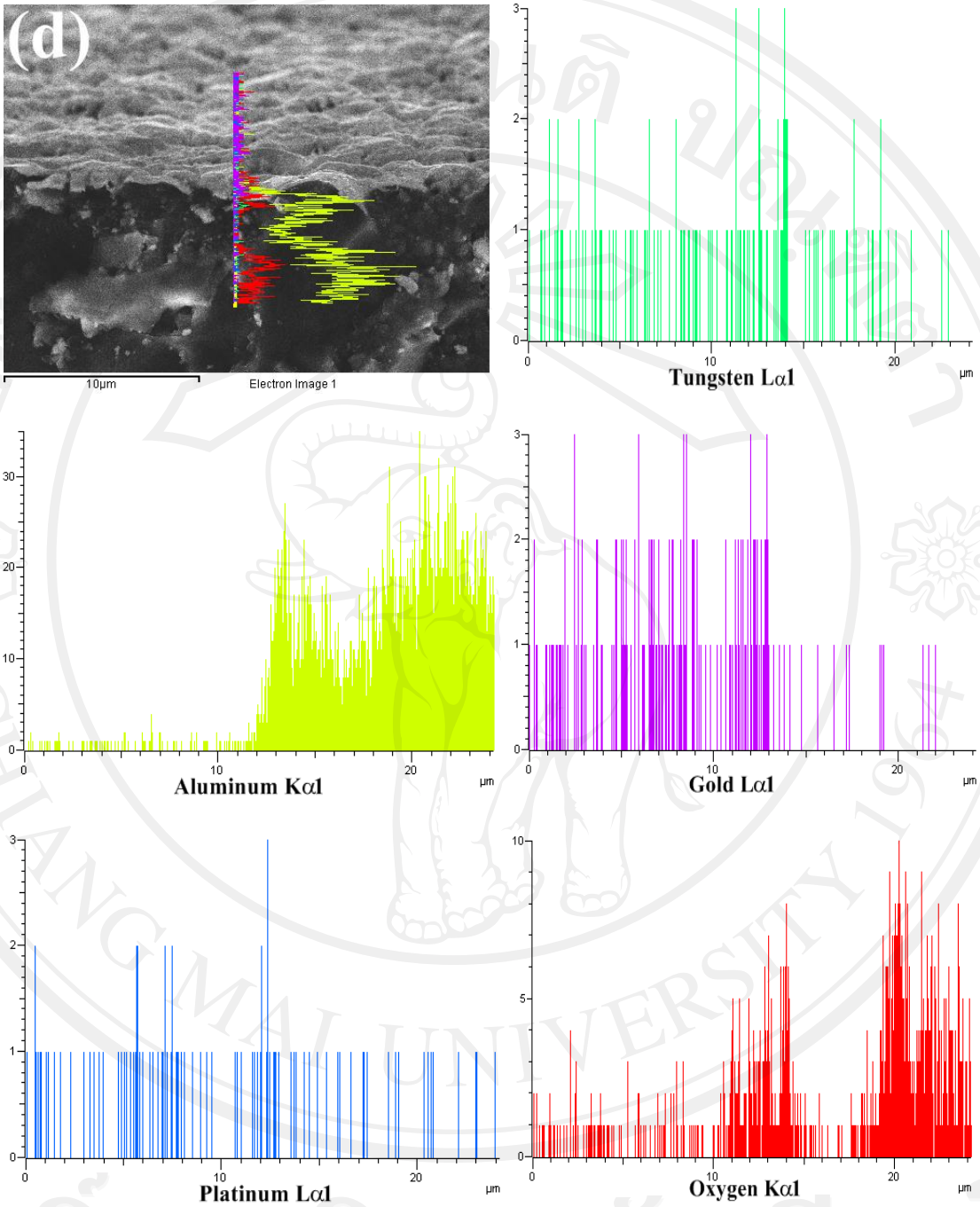

Figure 3.8 (d) The EDS line scan mode–SEM analysis of sensor (S1) based on 1.0 wt.% Pt-loaded WO_3 nanoparticles (H1). The histograms showed the elemental compositions of samples. The lines scans correspond to W, Al, Au, Pt and W elements.

3.2 Gas sensor based on Pt-loaded WO_3 nanoparticles (P0-P1)

3.2.1 Flammable and Explosive gases

3.2.1.1 Gas sensing of Pt-loaded WO_3 nanoparticles (P0-P1) synthesized by FSP towards hydrogen (H_2) gas

Hydrogen (H_2) is a clean, portable and potentially inexhaustible energy source with the potential to become a panacea for clean energy generation. However, H_2 has wide explosive concentration range (4–75 vol.%), low ignition energy (0.02 mJ) and large flame propagation velocity [147]. Due to its ultra small molecular size, confinement and containment of this gas are very difficult. Moreover, H_2 cannot be detected by human senses because it is colorless and odorless [148]. Thus, accurate detection and monitoring of hydrogen is an important issue.

The interaction of the resistive sensors with a target gas produces a change in the electrical conductance of the sensors recorded by a variation in the electrical resistance. Figure 3.9 (a)-(d) shows the change in resistance of sensors, S0-S1, under exposure to H_2 pulses with varying concentrations from 0.01 to 1 vol.% at 150–300^{o}C operating temperatures. The resistance reduction was clearly seen at all gas concentrations indicating that the WO_3 sensor had typical n-type semiconductor behaviors. It can be noticed that sensor, S1 (1.0% Pt), shows the best response with more drastic resistance change than sensors, S0.5 (0.5% Pt) and S0.25 (0.25% Pt), respectively while the sensor, S0 (0% Pt), gives no respond. Thus, small Pt loading can greatly improve H_2 response of WO_3 sensors. In addition, Pt-loaded WO_3 sensors have fast response with stable and full recovery even at low operating temperature of 150^{o}C. With increasing temperature, the response tends to be faster but the resistance change seems to be decreasing in all Pt-loaded sensors.

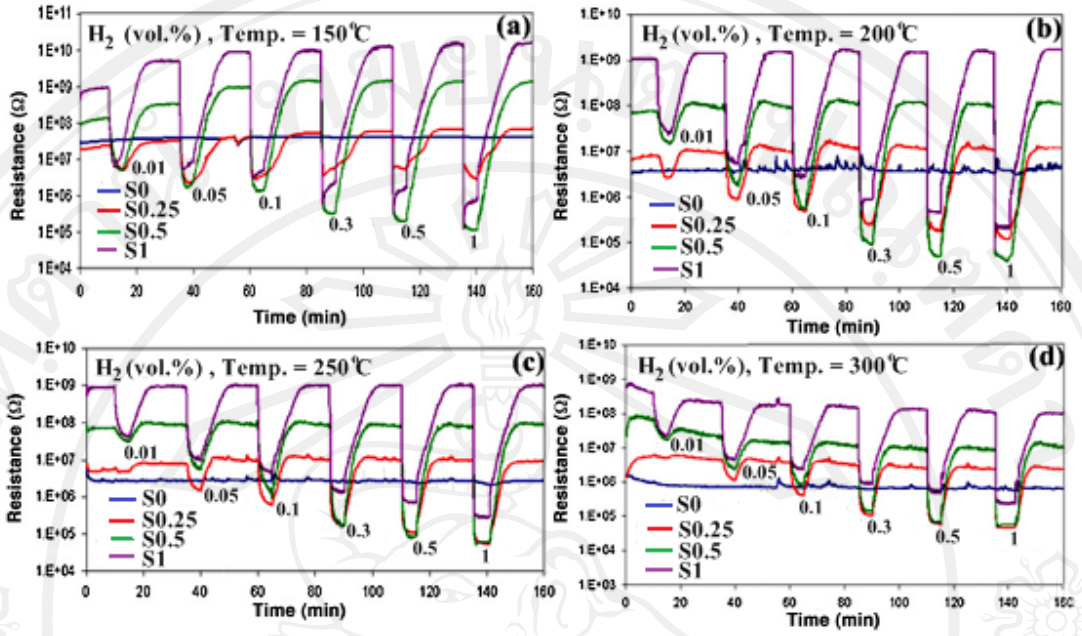

Figure 3.9 The change in resistance of sensors, S0-S1, under exposure to H_2 pulses with varying concentrations from 0.01 to 1 vol.% at 150–300°C (a-d), respectively.

The sensing behaviors were then analyzed in terms of gas-sensing response (S) and response time (T_{res}). S is defined as the ratio of R_a / R_g where R_a and R_g denoted the values of resistance of the films in dry air and tested gas, respectively while T_{res} is defined as the time required until 90% of the response signal is reached. Figure 3.10 demonstrates the gas-sensing response (left axis) and response time (right axis) versus H_2 concentration ranging from 0.01–1 vol.% for 1.0 wt.% Pt-loaded WO_3 sensor (S1) at operating temperature ranging from 150°C to 300°C. It can be seen that sensor, S1, shows the highest response and also with fast response time (within a few seconds) at low operating temperature of 150°C. As the temperature increases from 150 to 300°C, the response decreases by more than two orders of magnitude while the

response time remains roughly the same. Thus, the sensor exhibits very desirable behaviors of low operating temperature as well as fast response. In addition, the response of sensor, S1, increases drastically while response time decreases exponentially with increasing H_2 concentrations. In particular, a remarkably high response value of 1.34 x 10^5 was obtained at H_2 concentration of 1 vol.%.

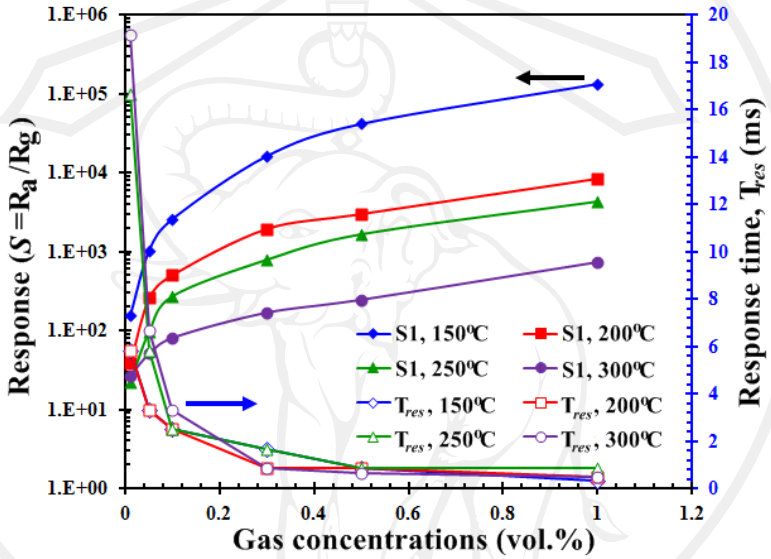

Figure 3.10 The response (left axis) and response time (T_{res}) (right axis) versus H_2 concentration ranging from 0.01–1 vol.% of the sensor, S1, at operating temperature ranging from 150–300°C.

The effect of operating temperature on H_2 response at 1 vol.% for WO_3 sensors with different Pt loading concentrations as shown in Figure 3.11. It can be seen that the H_2 response of unloaded WO_3 sensors was negligible at operating temperature up to 300°C. With a small of Pt content of 0.25 %, the hydrogen response increases by more than two orders of magnitude and optimum operating temperature was lower to ~250°C. As the Pt content increases to 0.5 and 1%, the response

increases by more than four and five orders of magnitude, respectively and the optimum operating temperature was further reduced to ~150°C. In addition, the H_2 response decreases monotonically as the operating temperature increases from 150°C to 300°C.

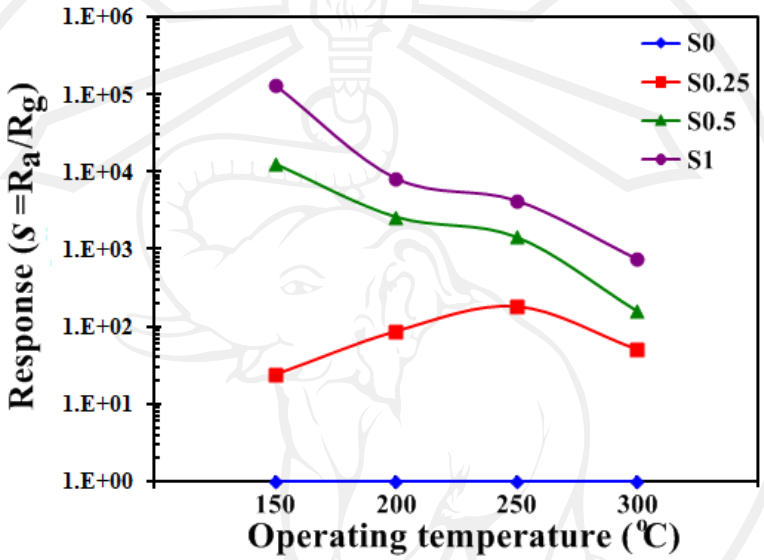

Figure 3.11 The response of sensors, S0-S1**,** versus operating temperature ranging from 150–300°C at 1 vol.% concentration of H_2.

From experimental results, unloaded WO_3 sensor shows almost no response to H_2 at operating temperature up to 300°C. This is in good agreement with other reports that reduction of unloaded WO_3 by hydrogen begins above 400°C [138, 149]. With Pt loading in the range between 0.25 to 1 %, H_2 response dramatically increases. The role of Pt in enhancing sensitivity and response rate of the sensor is known to be attributed to the chemical interaction between gas and sensitizer (Pt). Pt can dissociate H_2 into H atoms, which react with WO_3 support via the spillover process to from blue tungsten bronze by the following reactions [138, 146]:

$$0.5xH_2 \rightarrow xH_{ad} \quad (1)$$

$$xH_{ad} + WO_3 \rightarrow H_xWO_3 \quad (2)$$

WO_3 was a greenish yellow crystalline solid. The reaction accompanies remarkable change in color. This reaction may occur even at room temperature because of very low activation energy between the Pt modified surface and the target gas [149−151]. It has been known that the reaction was partially reversible. However, the reaction may be almost irreversible for some preparation methods and experimental conditions of Pt-loaded WO_3. Therefore, oxidizing agent, such as oxygen, was needed for the reformation of WO_3 matrix [152, 153]. The reformation reaction is described as follow:

$$H_xWO_3 + 0.25xO_2 \rightarrow WO_3 + 0.5xH_2O \quad (3)$$

According to the spillover effect, adsorbed reactants will migrate to the oxide surface to react there with surface oxygen species, affecting the surface conductivity. The electrical resistance of Pt/WO_3 nanoparticles was effectively controlled by the reaction via the depletion layer modulation at the metal-semiconductor (Pt/WO_3) contacts. The depletion layer width was controlled by a potential barrier at Pt/WO_3 interface that was fully characterized by the electron affinity of WO_3, the work function of Pt and the surface state density of WO_3 within the energy gap. For a metal with high work function like Pt, large barrier height results in a wide depletion region. When reacted to H atom, the barrier height at junction decrease due to electron transfer, resulting in larger resistance reduction than the case of unloaded WO_3 nanoparticles. For the above processes to be effective, catalyst should be very small in size but large in number and uniformly dispersed so that reactant species were available near all interparticle contacts and effectively control interparticle contact

resistance. The effect can be further enhanced greatly by larger specific surface area of sensing surface.

According to the results, FSP prepared Pt/WO_3 sensors provide much higher H_2 response compared to those of other reports. The attribute of this extraordinary response by two contributions. Firstly, Pt-loaded WO_3 material produced by FSP contains a large number of sub-nanometer Pt particles that was well dispersed in and on WO_3 nanoparticles. Thus, spill-over mechanism was highly effective in this structure, resulting in a great enhancement of H_2 response. Secondly, Pt-loaded WO_3 film prepared by FSP and spin coating had a huge specific surface area owing to its nano-porosity and moderately large thickness of 30 μm. From these contributions, the H_2 response of Pt-loaded WO_3 film in the present work was a few orders of magnitude larger than those of other reports based on Pt-WO_3 thin film gas sensors, which the highest response of 200 was obtained at 1 vol.% H_2 concentration [13, 93, 127].

Regarding the influence of Pt loading concentration, H_2 response of FSP prepared Pt/WO_3 film monotonically increases with Pt loading concentration up to 1.0 wt.% and the ultimate optimal Pt content for H_2 sensing was expected at a higher Pt loading content. Further study will be conducted to determine the actual optimal Pt content in FSP prepared Pt/WO_3 nanoparticles for H_2 sensing. However, it should be noted that 1.0 wt.% Pt loading was chosen as the limit of this study because other reports found the optimal Pt loading concentration of 0.4–0.5% for H_2, CO and C_2H_5OH gases [138, 139]. The different optimal Pt loading concentrations could be due to different sizes and dispersions of Pt particles formed by distinct preparation methods. For screen printed and sputtered Pt/WO_3 films, relatively large Pt nanoparticles began to agglomerate and poorly disperse at low Pt concentrations of

more than 0.4–0.5% [138, 139]. As a result, H_2 response degraded at concentrations higher than these optimal values. In contrast, our results demonstrate that FSP method produces sub-nanometer Pt particles that were very well dispersed in WO_3 nanoparticles at Pt loading concentration up to 1 %. Therefore, optimal Pt concentration of Pt-loaded WO_3 nanoparticles synthesized by FSP was higher than those prepared by other methods because much smaller and more uniformly dispersed Pt nanoparticles were produced even at the higher Pt concentrations.

For the effect of operating temperature, it was seen that the FSP prepared Pt-loaded WO_3 films exhibits optimum H_2 response at low temperature of 150^{o}C and the response considerably decreased as operating temperature increased. This result was similar to some Pt/WO_3 films prepared by other methods [127, 139] but this behavior was in contrast to other Pt-loaded metal oxides such as Pt/ZnO, in which H_2 response increased with operating temperature ranging from 200–350^{o}C [154]. The mechanism for such negative temperature dependence of hydrogen response for Pt/WO_3 films, which has not been clearly explained in the literature, was proposed based on the model in Figure 3.12. In this model, Pt particles were assumed to be very small in subnanometer scale in accordance with our experimental observation. At a low temperature (i.e.150^{o}C) (Figure 3.12 (a)), adsorbed oxygen species (mostly O^{-}) have low density and spillover effect was effective as usual. At a high temperature (i.e., 250–300^{o}C) (Figure 3.12 (b)), the number of adsorbed oxygen species increases significantly and some of them locate around the subnanometer Pt particles. These adsorbed oxygen species shield Pt particles from H_2 and reduce probability of H_2 dissociation by Pt. Thus, H_2 response decreases considerably because the spillover effect by Pt is substantially hindered while the rate of direct hydrogen reduction by

WO_3 is still very low. The shielding effect will not be significant if Pt particle is considerably larger than adsorbed oxygen species and this was seen to be the case for Pt/ZnO synthesized by FSP, in which Pt nanoparticles were found to be larger than 1 nm [154].

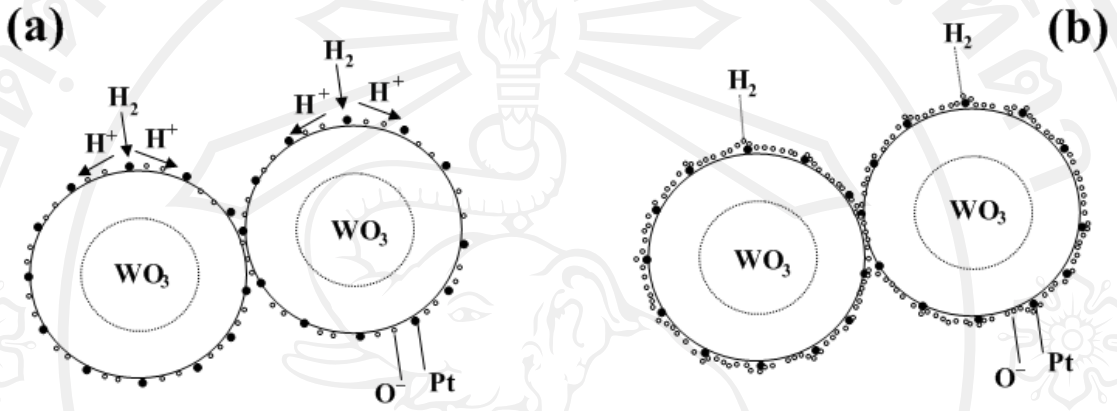

Figure 3.12 Model of Pt-loaded WO_3 for explanation of the effect of operating temperature on hydrogen sensing: (a) low operating temperature (i.e., 150^{o}C) and (b) high operating temperatures (i.e., 250–300^{o}C).

From the data, it can be seen that sensor S1 showed the highest response value of 1.34 x 10^5 at 150^{o}C towards 1 vol.% H_2. When compared H_2 response of sensor with the same material, Penza *et al.* [13] reported Pt-loaded WO_3 sensor was prepared by reactive rf sputtering. At the operating temperature 150^{o}C, Pt-loaded WO_3 showed maximum response of 3.45 towards 0.05 vol.% H_2. In addition, Pt-loaded WO_3 sensor prepared by R.F. magnetron sputtering was reported by Ippolito *et* al. [127]. It was found that sensor shows highest response of ~200 towards 1 vol.% H_2 at 150^{o}C. Moreover, when compared with another material which prepared by FSP (nanoparticles) and spin coating (sensors). It was clearly seen that 0.2 at.% Pt-loaded ZnO thick film exhibited response of ~164 for 1 vol.% H_2 at 300^{o}C [155]. Thus, the

results indicate that Pt-loaded WO_3 prepared by FSP gave much higher H_2 response when compared to those of other reported.

3.2.1.2 Gas sensing of Pt-loaded WO_3 nanoparticles (P0-P1) synthesized by FSP towards ethanol (C_2H_5OH) gas

Ethanol (C_2H_5OH) is a colorless liquid with a characteristic, agreeable odor. In dilute aqueous solution, it has a somewhat sweet flavor, but in more concentrated solution, it has a burning taste. Detection of ethanol vapor is an important feature of the breath alcohol content or even to detect leaks in industrial lines. Ethanol detection is primarily in the range of 10–5000 ppm for monitoring human blood alcohol level and its TLV is 1000 ppm [156]. In addition, ethanol concentration is sometimes measured near its explosive range of 3–19 vol.%.

The C_2H_5OH gas-sensing properties of unloaded WO_3 (S0) and 0.25–1.0 wt.% Pt-loaded WO_3 sensors (S0.25-S1) were tested. It is well known that rate of gas response (The gas–sensing response, S is defined as the ratio R_a/R_g) to C_2H_5OH was much dependent on the operating temperature and the amounts of additives. Such tendencies were shown in Figure 3.13. It can be seen that response of these sensors to 1000 ppm C_2H_5OH varies with only the operating temperature but also the concentration of Pt. In the range of the operating temperatures studied, from 150 to 300^oC, the response values increased sharply at first and gradually decreased for all the sensors. Each curve presents a maximum at an optimal operating temperature. The unloaded WO_3, 0.5 and 1.0 wt.% Pt-loaded WO_3 sensors have the maximum gas response which were estimated to be 4.48, 1.3 x 10^3 and 2.4 x 10^3 at 200^oC, while 0.25 wt.% Pt-loaded WO_3 sensor has the maximum gas response which was observed

to be 259 at 250°C. The sensor response and operating temperature of Pt-loaded WO_3 sensor were the highest response and lower temperature. Furthermore, the Pt-loaded sensors exhibit much higher response than the unloaded WO_3. Especially, the 1.0 wt.% Pt-loaded WO_3 sensor presents the largest response towards C_2H_5OH at 200°C.

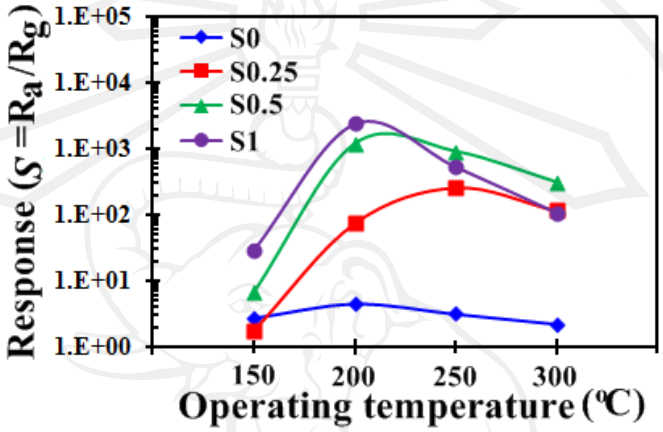

Figure 3.13 Response of unloaded WO_3 and Pt-loaded WO_3 sensors operated at 150–300°C towards 0.1 vol.% C_2H_5OH.

Figure 3.14 demonstrates the response of unloaded and Pt-loaded WO_3 sensors to different concentrations of C_2H_5OH (0.005–0.1vol.%) measured at the same operating temperature of 200°C. It can be seen that the gas response of the loaded sensors is higher than that of the unloaded WO_3. And the response values of the sensors increased drastically while response time decreases exponentially with an increase of the C_2H_5OH gas concentration. Thus, it was obvious from Figure 3.14 that not only temperature but also C_2H_5OH concentration plays a role in determining the response of the sensing films.

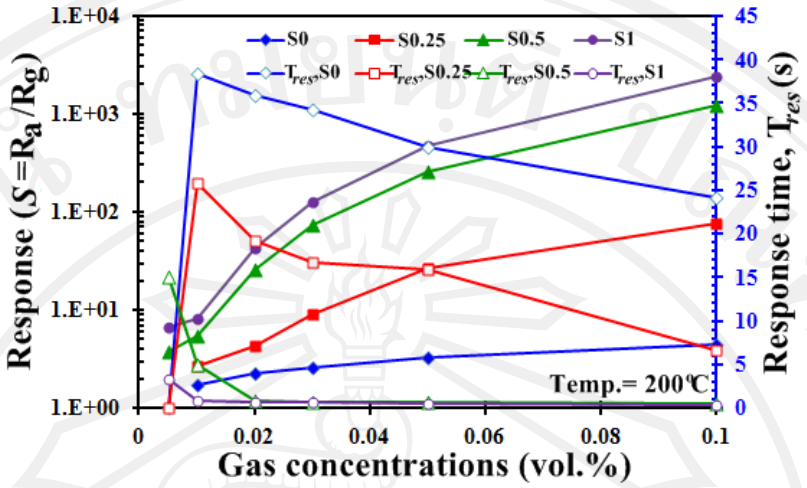

Figure 3.14 Response (left axis) and response time (T_{res}) (right axis) of unloaded WO_3 and Pt-loaded WO_3 sensors to different concentration of C_2H_5OH at 200°C.

From experimental results, it was obvious that sensor S1 showed the highest response value of ~$2.4x10^3$ at 200°C towards 0.1 vol.% C_2H_5OH. When compared C_2H_5OH response of sensor with the same material, Zhang *et al.* [88] reported Pt-loaded WO_3 (powders) and sensor were prepared by the coprecipitation and spin coating, respectively. At the operating temperature of 140°C, 2.36 wt.% Pt/WO_3 sensors showed maximum response of ~87.1 toward 0.01vol.% C_2H_5OH. In addition, unloaded WO_3 sensor prepared by screen-printing was reported by Khadayate *et al.* [129]. It can be seen that sensor shows highest response of ~1424.6 towards 50 ppm C_2H_5OH at 400°C. However, 0.4 wt.% Pt/WO_3 sensor was prepared by screen-printing showed very low response of ~2 towards 0.016 vol.% C_2H_5OH at 450°C as reported by Srivastava *et al.* [138]. Moreover, when compared with another material which prepared by FSP (nanoparticles) and spin coating (sensors). It was found that 0.5 mol% W-loaded ZnO thick film exhibited response of ~6 for 0.01vol.% C_2H_5OH

at 400^{o}C [157]. Thus, the results indicate that Pt-loaded WO_3 prepared by FSP demonstrated much higher C_2H_5OH response as compared to those of other reported.

3.2.1.3 Gas sensing of Pt-loaded WO_3 nanoparticles (P0-P1) synthesized by FSP towards carbon monoxide (CO) gas

Carbon monoxide (CO) is a colorless and odorless gas, making it undetectable to human [158]. It is mainly produced due to the incomplete combustion of fuels and commonly found in the emission of automobile exhaust. The gas has been shown to bind irreversibly to the iron center of hemoglobin, the oxygen transport molecule in blood. Thus, oxygen can no longer be absorbed and high levels of CO exposure will result in death. CO is mainly of interest as toxic gases and its detection range of interest is typically 1−1,000 ppm because its TLV is 25 ppm. However, CO is also explosive and there is some interest for its measurement in the high concentration range near its minimum explosive limit of 12.5 vol.%.

The temperature has an obvious influence on the response of sensors to CO gas (The gas-sensing response, S is defined as the ratio R_a/R_g). In order to determine the optimal operating temperatures, the response of 1.0 wt.% Pt-loaded WO_3 (S1) sensors with concentrations to 0.1 vol.% of CO in air was tested as a function operating temperature, as shown in Figure 3.15. It can be seen that response of sensor S1 increased with temperature, up to 200^{o}C, and then gradually decreased. Therefore, optimal operating temperature of 200^{o}C was chosen for CO.

Figure 3.16 shows the gas-sensing response (left axis) and response time (right axis) versus CO concentration ranging from 0.005–0.1 vol.% for the unloaded (S0) and Pt-loaded WO_3 sensor (S0.25-S1) at operating temperature of 200^{o}C. It can be

seen that the response of sensor S1 increases drastically while response time decreases exponentially with increasing CO concentrations. In particular, a high response value of ~1.2 x10^2 was obtained at CO concentration of 0.05 vol.%.

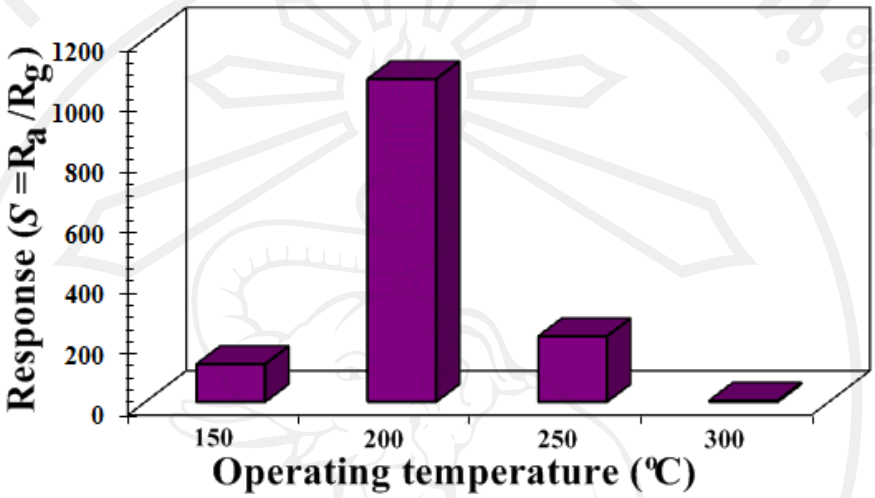

Figure 3.15 The response of 1.0 wt.% Pt-loaded WO_3 (S1) sensors versus operating temperature ranging from 150–300°C at 0.1 vol.% concentration of CO.

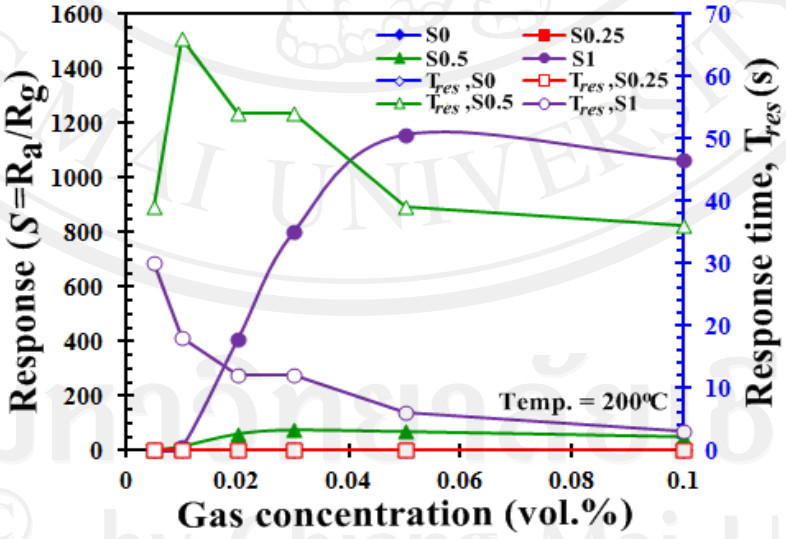

Figure 3.16 The response (left axis) and response time (T_{res}) (right axis) versus CO concentration ranging from 0.005–0.1 vol.% of the sensor, S0-S1, at operating temperature ranging from 200°C.

According to the results, it can be seen that sensor S1 showed the highest response value of ~1.2 x10^2 at 200^{o}C towards 0.05 vol.% CO. When compared CO response of sensor with the same material, Penza *et al.* [13] reported unloaded and Pt-loaded WO_3 sensors showed the same response of ~0.05 towards 0.1 vol.% CO at 250 ^{o}C and 150^{o}C, respectively. Therefore, Pt catalyze was not able to increase the response but can reduce the operating temperature. Pt-loaded WO_3 sensor prepared by sputtering was reported by Tao *et al.* [14]. It was found that sensor show the highest response of ~2.3 towards 0.01 vol.% CO at 220^{o}C. In addition, Srivastava *et al.* [138] reported 0.4 wt.% Pt/WO_3 sensor was prepared by screen-printing showed response of ~1.5 toward 0.08 vol.% CO at 450^{o}C. Furthermore, when compared with another material which prepared by FSP (nanoparticles) and followed by spin coating (sensors). It was seen that 2 at.% Pt-loaded ZnO thick films showed response of ~2.4 for 0.1vol.% CO at 300^{o}C [155]. Finally, 0.5 mol% Nb-loaded ZnO sensor exhibited response of ~2.8 for 0.1vol.% CO at 400^{o}C [159]. Therefore, the results indicate that Pt-loaded WO_3 prepared by FSP demonstrated much higher CO response when compared to those of other had reported.

3.2.1.4 Gas sensing of Pt-loaded WO_3 nanoparticles (P0-P1) synthesized by FSP towards ethylene (C_2H_4) gas

Ethylene (C_2H_4) is a colorless flammable gas with a sweet odor. The chemical properties of C_2H_4 result from the carbon-carbon double bond, with a bond length of 0.134 nm and its planar structure [160]. C_2H_4 is a very reactive intermediate, which can undergo all typical of reactions with a short-chain olefin, making it an important chemical building block and its production involves complicated separation process.

C_2H_4 can be converted to saturated hydrocarbons, oligomers, polymers, and derivatives thereof. Chemical reactions of ethylene with commercial importance include addition, alkylation, halogenation, hydroformylation, hydration, oligomerization, oxidation, and polymerization. Moreover, ethylene is naturally produced from ripening agricultural products and its detection range of interest is 0.1–100 ppm (TLV = 1 ppm) for monitoring their freshness. In addition, ethylene concentration is often measured in the range near its minimum explosive limit of 3 vol.%.

The response and response times of the sensing films of WO_3 nanoparticles as a function of C_2H_4 concentration between 0.005 and 0.1 vol.% at 150°C were shown in Figure 3.17 (a) (The gas-sensing response, S is defined as the ratio R_a/R_g). The response was increased considerably by loading 1.0 wt.% Pt-loaded WO_3. The response value of 9.9 and response time of 114 s were obtained at 0.1 vol.% of C_2H_4 concentration present for 1 wt.% Pt. The response, however, was decreased considerably when loading the 0.5 and 0.25 wt.% Pt-loaded WO_3. It was important to note that the unloaded WO_3 and Pt-loaded WO_3 nanoparticles behave as an n-type semiconductor with the resistance decreased during C_2H_4 gas environment as shown in Figure 3.17 (b). The semiconducting and gas-sensing behaviors were thus strongly depending on the loading level of Pt on WO_3 nanoparticles.

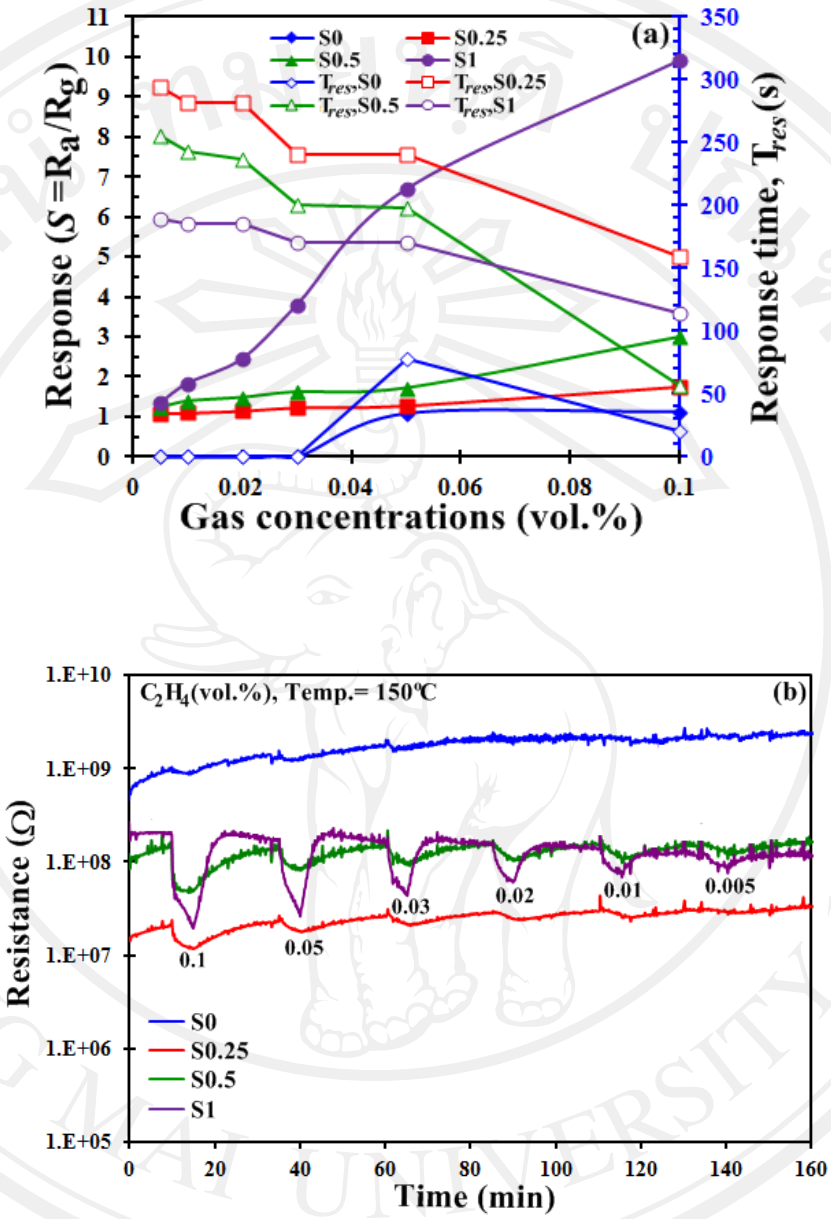

Figure 3.17 (a) Variation of response (left axis) with concentration of C_2H_4 (0.005–0.1 vol.%) and variation of response times (right) for S1, S2, S3 and S4 at 150°C. (b) Change in resistance of sensors, S0-S1, under exposure to reducing gas C_2H_4 pulses during forward cycle.

From the data, it was obvious that sensor S1 showed the highest response value of ~9.9 at 150°C towards 0.1 vol.% C_2H_4. When compared C_2H_4 response of sensor with the same material, Nimittrakoolchai *et al.* [23] reported unloaded WO_3 sensor was prepared by precipitation method. At the operating temperature of 300°C, sensing film showed maximum response of ~4.5 towards 10 ppm C_2H_4. In addition, when compared with another material which prepared by FSP (nanoparticles) and spin coating (sensors). The 0.2 at.% Pt-loaded ZnO thick film exhibited response of ~0.89 for 1 vol.% C_2H_4 at 350°C [157]. Therefore, the results indicated that Pt-loaded WO_3 prepared by FSP demonstrated much higher C_2H_4 response when compared to previously known reporteds.

3.2.2 Atmospheric pollution gas

3.2.2.1 Gas sensing of Pt-loaded WO_3 nanoparticles (P0-P1) synthesized by FSP towards nitrogen dioxide (NO_2) gas

Nitrogen oxides (NO_x) are crucial points to reduce the noxious effects on environment and human beings. Two of the most toxicologically significant nitrogen oxides are nitric oxide (NO) and nitrogen dioxide (NO_2); both are non-flammable and colorless to brown color at room temperature. NO is a sharp sweet-smelling gas at room temperature, whereas NO_2 has a strong, harsh odor and is a liquid at room temperature. Among them, NO_2 is the most hazardous gas with TLV of 3 ppm [161]. NO_2 is created by the high temperature combustion of coal, chemical production, natural gas or oil in power plants and also by the combustion of gasoline in internal combustion engines. One of the consequences of NO_2 released into the atmosphere is

the formation of photochemical smog. In addition, NO_2 is a cause of acid rain and is involved in the depletion of ozone in the stratosphere [162].

Figure 3.18 illustrates the change in resistance of sensors, S0-S1, under exposure to NO_2 gas with different concentrations ranging from 1 to 50 ppm at 150°C. The increase of resistance was clearly specified at all gas concentrations indicating that the WO_3 sensor had typical n-type semiconductor behaviors. However, the increase in resistance was small and the recovery speed was slow for pure WO_3 material. Adsorption of NO_2 on WO_3 nanoparticles results in a decrease of the conductivity, which may be explained by the following reactions [111]

$$NO_2\,(g) + e^- \leftrightarrow NO_2^-\,(ads) \qquad (4)$$

$$NO_2\,(g) + e^- \leftrightarrow NO(g) + O^-\,(ads) \qquad (5)$$

Both of these reactions require electrons from the conduction band of WO_3, which then lead to a decrease of the conductivity.

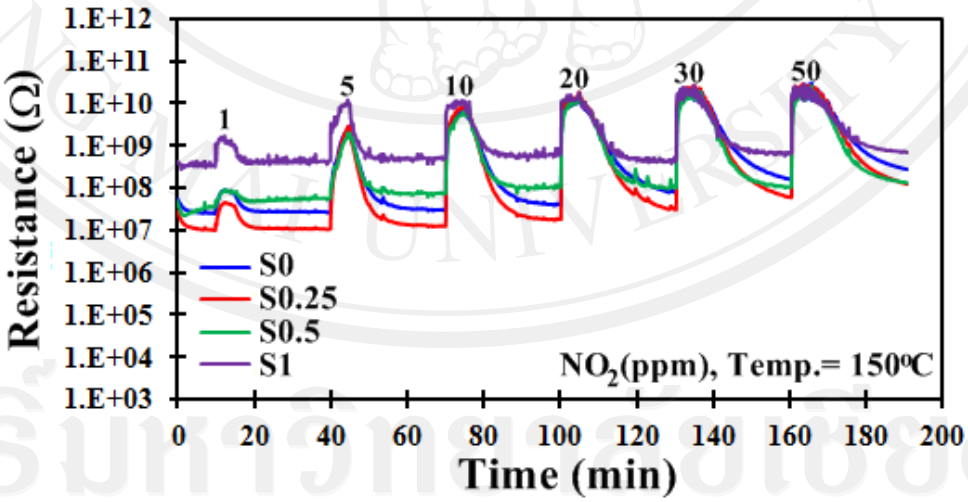

Figure 3.18 The change in resistance of sensors, S0-S1, under exposure to NO_2 pulses with different concentrations ranging from 1 to 50 ppm at 150°C.

The response of unloaded WO_3 (S0) thick film was of 327 and observed towards 20 ppm at 150°C as shown in Figure 3.19. On loading with Pt catalysts the gas response was enhanced. It can be seen that sensor S0.25 (0.25%Pt) showed the best response than sensor S0.5 (0.5%Pt) and S1 (1.0%Pt). In addition, the response of sensor S0.25 (0.25%Pt) was about 954 towards 20 ppm NO_2 at 150°C. The response time of NO_2 became less than 2 min. Thus, small Pt loading could greatly improve response towards NO_2.

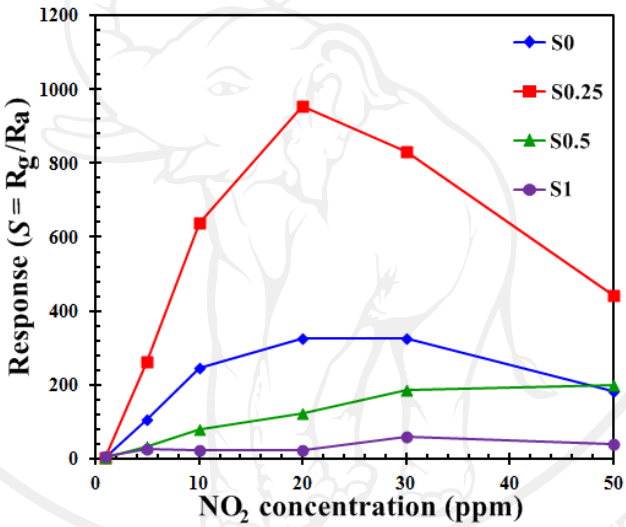

Figure 3.19 The relative of response with concentration of NO_2 (ppm) between unloaded WO_3 (S0) and 0.25–1.0 wt.% Pt-loaded WO_3 sensors (S0.25-S1) at 150°C.

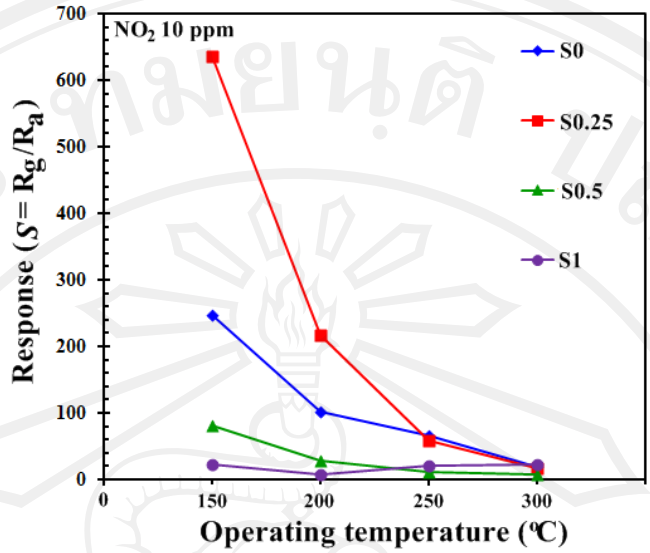

Figure 3.20 Response versus operating temperature curve for unloaded WO_3 (S0) and 0.25–1.0 wt.% Pt-loaded WO_3 sensors (S0.25-S1).

The effect of operating temperature on NO_2 response at 10 ppm for WO_3 sensors with different level of Pt loading concentrations is shown in Figure 3.20. It can be seen that the all sensors showed the high response at low operating temperature of 150°C and the response considerably decreases as operating temperature increases. Therefore, optimal operating temperature of 150°C was chosen for NO_2. This is in agreement with other reports that the temperature for the maximum response to NO_x corresponds to about 150°C for Pt/WO_3 [13]. From the experimental results, it was found that sensor S0.25 showed the highest response value of 637 at 150°C towards 10 ppm NO_2. Comparing with the same material, Penza *et al.* [13] reported that the highest sensing behaviors of Pt-loaded WO_3 to 10 ppm NO_2 was about 3.45 at 150°C. Srivastava *et al.* [138] reported the Pt-loaded WO_3 film prepared by screen-printing, and the sensing test at 450°C with NO_2 at concentration ranging from 40–400 ppm. A sensor showed the highest sensor signal

at 400 ppm (S = ~4). Stankova *et al.* [143] also reported Pt-loaded WO_3 sensor prepared by reactive r.f. sputtering with response of 11.73 to 10 ppm NO_2 at 260^oC. However, when compared with another material which prepared by FSP (nanoparticles) and spin coating (sensors). It was found that 0.5 mol% Nb/ZnO thick film exhibited response of ~1640 and a short response time (27s) for 4 ppm NO_2 at 300^oC [159].

3.2.3 Selective gas sensors based on flame-spray-made Pt-loaded WO_3 nanoparticles

To quantitatively determine the selectivity of sensors, the responses towards H_2, C_2H_4, C_2H_5OH, and CO of all sensors were calculated and plotted at the fixed concentration of 0.1 vol.% and operating temperature of 150^oC as shown in Figure 3.21. The figure shows that sensor, S1, exhibits very high H_2 response but much weaker responses to CO, C_2H_5OH and C_2H_4, respectively. The results indicate that Pt loading improves selectivity towards H_2 for WO_3 sensors. From the data, sensor S1, has the response values towards H_2, CO, C_2H_5OH and C_2H_4, of 2.58 x 10^3, 124, 29 and 9.9, respectively at 0.1 vol.% concentration of testing gas at 150^oC operating temperature. Thus, the sensor has the H_2 selectivity relative to CO, C_2H_5OH and C_2H_4 of 20.8, 88.9 and 260, respectively. The selectivity was defined as the ratio of H_2 response to that of another gas. The H_2 selectivity relative to CO was relatively low compared to other gases because Pt was a catalyst for CO reduction. Nevertheless, this selectivity value was still good for some applications.

Finally, reproducibility and stability of sensors were assessed. Five sensors from the same batch were found to have response variation of less than 15 %. The sensors also exhibit good stability with less than 20 % drift in response over 1 month operation.

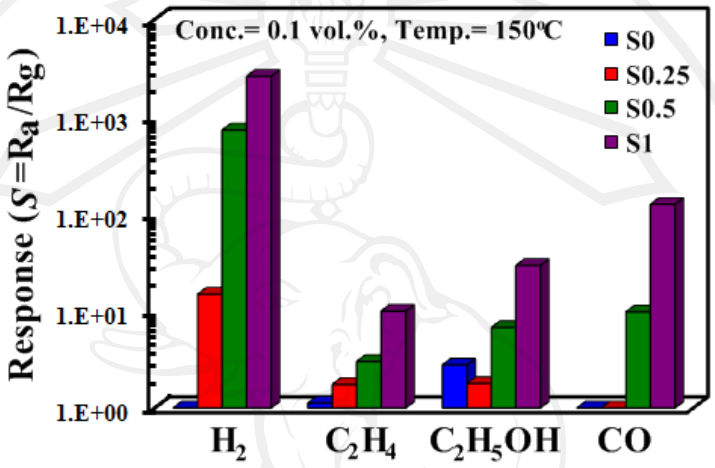

Figure 3.21 The selectivity histograms of unloaded WO_3 (S0) and 0.25–1.0 wt.% Pt-loaded WO_3 sensors (S0.25-S1) for flammable and explosive gases at concentration of 0.1 vol.% and operating temperature of 150°C.

3.3 Gas sensor based on Pt-loaded WO_3 nanoparticles (H0-H1)

3.3.1 Flammable and Explosive gases

3.3.1.1 Gas sensing of Pt-loaded WO_3 nanoparticles (H0-H1) synthesized by hydrothermal towards hydrogen (H_2) gas

The gas-sensing response (S) of the sensing films of WO_3 nanoparticles was defined as the ratio R_a/R_g. Figure 3.22 shows the response of the unloaded WO_3 (S0) and 1.0 wt.% Pt-loaded WO_3 (S1) films to 1 vol.% H_2 at varying operating temperatures. The response of the films increases as the operating temperature increases up to 250°C, and then declines. At any operating temperature, the sensor

response of the 1.0 wt.% Pt-loaded WO_3 (S1) film is higher than that of the unloaded WO_3 film. Specifically, at the optimum operating temperature (250^oC), the response of the 1.0 wt.% Pt-loaded WO_3 (S1) film showed approximately 211 time more response than that the unloaded WO_3 film (S0).

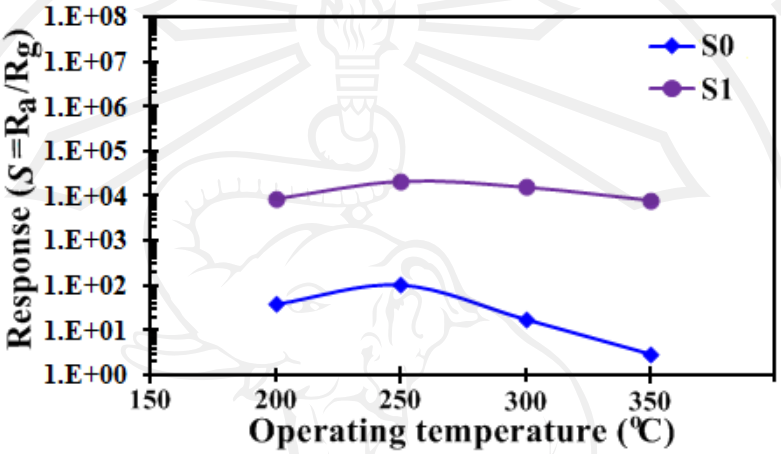

Figure 3.22 Sensing response to H_2 (1 vol.%) at different operating temperatures.

One major advantage of Pt-loaded WO_3 films were that the sensors can be operated at lower operating temperature (250^oC), especially, if these sensors were used to measure the H_2 gas at higher concentrations (1 vol.%) . The response was increased considerably by loading 1.0 wt.% Pt-loaded WO_3. The response value of 2.16 x 10^4 and response time of 0.0252 s were obtained at 1 vol.% of H_2 concentration. The response, however, was decreased considerably when the 0.5 and 0.25 wt.% Pt-loaded WO_3 as shown in Figure 3.23. From the data, there were sufficient numbers of H_2 molecules available to react with the surface oxygen adsorption sites. It was also well-known that Pt nanoparticles contribute to the reduction of sensors resistance of metal oxides and the activation energy between the WO_3 surface and H_2 gas.

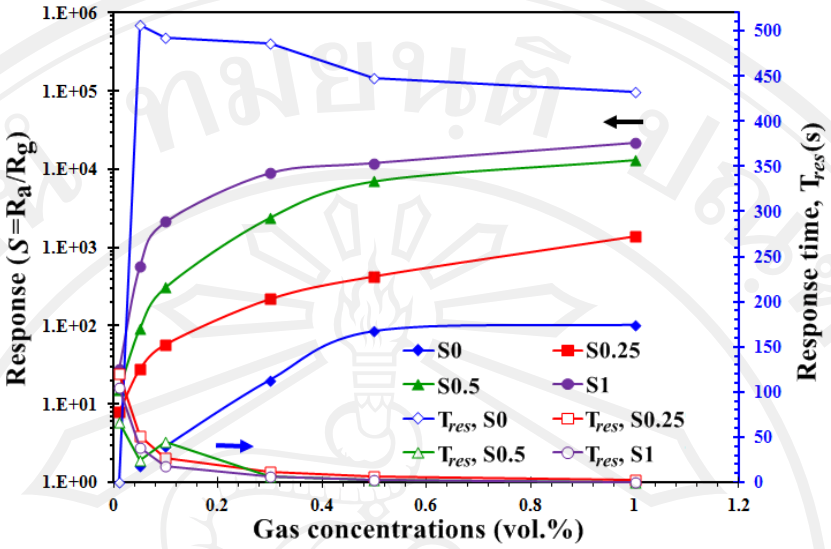

Figure 3.23 Sensing response of the unloaded WO_3 (S0) and 0.25–1.0 wt.% Pt-loaded WO_3 sensors (S0.25-S1) to H_2 concentrations (0.01–1 vol.%) at the operating temperature of 250°C.

According to the results, it can be seen that sensor S1 showed the highest response value of ~2.16 x 10^4 at 250°C towards 1 vol.% H_2. When compared H_2 response of sensor with the same material, Shen *et al.* [93] reported that unloaded WO_3 sensor was prepared by reactive magnetron sputtering. At the operating temperature of 300°C, the sensor showed maximum response of ~13.6 towards 0.1 vol.% H_2. In addition, 0.5 at.% Pt-loaded WO_3 sensor prepared by radio frequency sputtering was reported by Zhang *et al.* as well [139]. It was obvious that sensing film showed highest response of ~26 towards 0.02 vol.% H_2 at 95°C. When compared with another sensing material, Liewhiran *et al.* [163] reported 0.2 wt.% Ru-loaded SnO_2 nanoparticles synthesized by FSP and sensor was prepared by spin coating. It was found that sensing film showed response of ~27 for 1 vol.% H_2 at 350°C. Therefore,

the results indicate that Pt-loaded WO_3 prepared by hydrothermal gave a much higher H_2 response as compared to those of other reported.

3.3.1.2 Gas sensing of Pt-loaded WO_3 nanoparticles (H0-H1) synthesized by hydrothermal towards ethanol (C_2H_5OH) gas

The dependence of the C_2H_5OH gas-sensing response ($S=R_a/R_g$) on the operating temperature as shown in Figure 3.24. The 0.1 vol.% C_2H_5OH gas response presents a maximum value at 350°C. The 1.0 wt.% Pt-loaded WO_3 sensor (S1) gas response increases from 250 to 1406 when the temperature changes from 200 to 350°C. The optimum operating temperature has been selected at 350°C and this temperature will be fixed for further studies through out the sensor gas response as a function of the gas concentration.

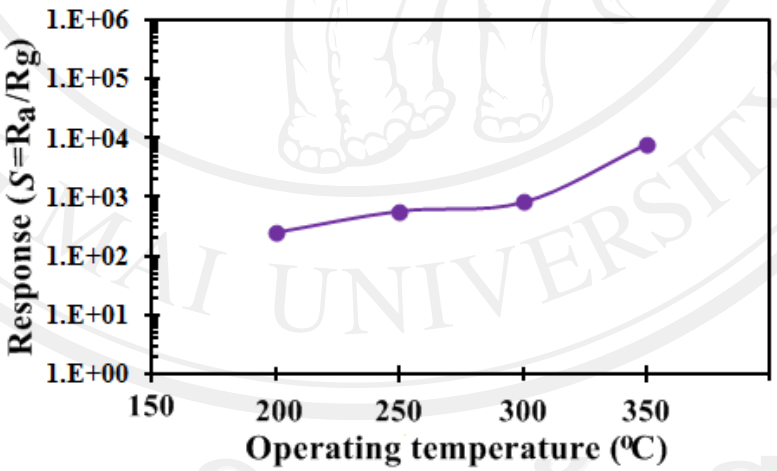

Figure 3.24 Gas sensing response of 1.0 wt.% Pt-loaded WO_3 (S1) sensor to 0.1 vol.% C_2H_5OH as a function of operating temperatures.

The gas response of sensing films to different concentration of C_2H_5OH has been evaluated at 350°C as shown in Figure 3.25. The response was increased considerably by loading the sensing films with Pt. It can be noticed that sensor, S1 (1.0% Pt), shows the best response with more than other sensors, S0.5 (0.5% Pt) and S0.25 (0.25% Pt), respectively. Two behavior regions can be distinguished: in the first one (between 0.005 and 0.05 vol.%) the gas response increases slowly 5.6 to 319, while between 0.05 and 0.1 vol.% C_2H_5OH the gas response increases much faster, i.e., from 319 to 1406. Figure 3.26 shows a typical characteristic for the unloaded WO_3 and Pt-loaded WO_3 films as an n-type semiconductor with the resistance decreased upon expose to C_2H_5OH gas.

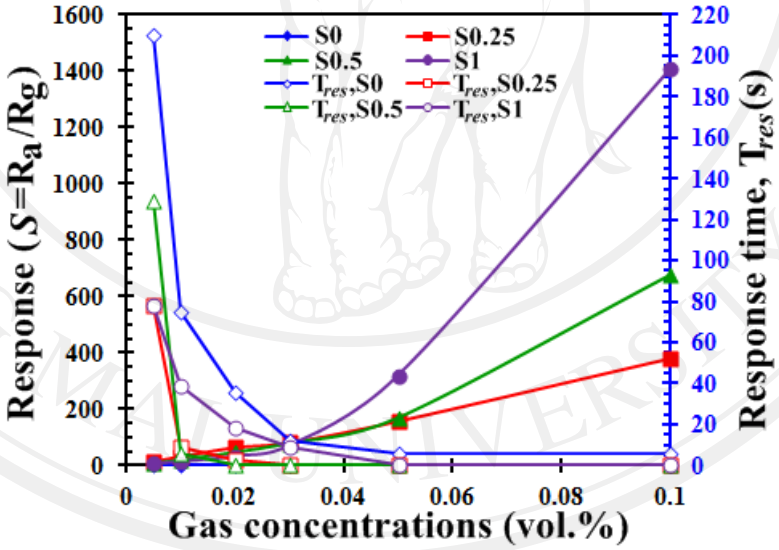

Figure 3.25 Gas sensing response of 1.0 wt.% Pt-loaded WO_3 (S1) sensor as a function of C_2H_5OH concentration at 350°C operating temperature.

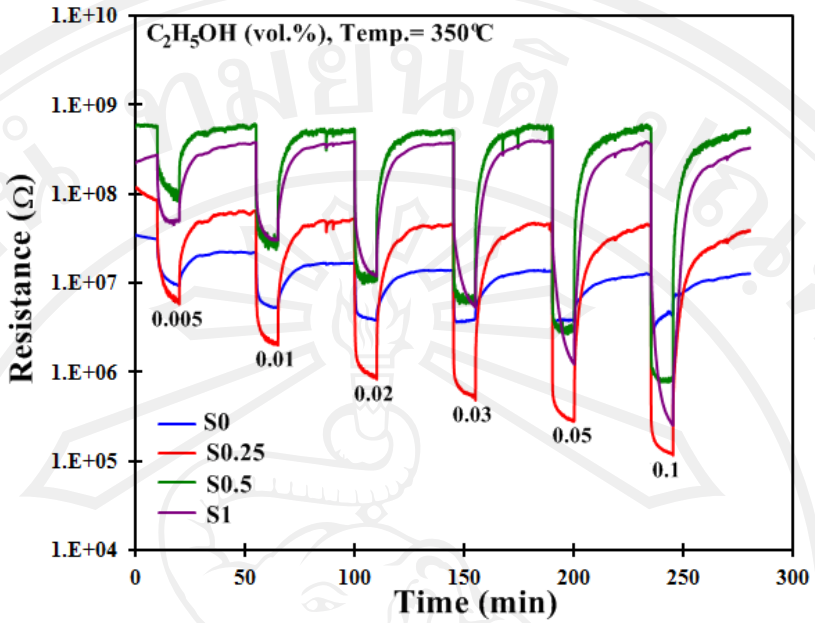

Figure 3.26 Change in resistance of sensing films upon exposure to C_2H_5OH in forward cycle at 350°C.

From the data, it was found that sensor S1 showed the highest response value of ~1406 at 350°C towards 0.1 vol.% C_2H_5OH. When compared C_2H_5OH response of sensor with the same material, Su *et al.* [164] reported unloaded WO_3 (powders) and sensor which prepared by hydrothermal and followed with spin coating, at the operating temperature of 340°C, their sensor showed maximum response only ~5 toward 0.05vol.% C_2H_5OH. In addition, unloaded WO_3 powders prepared by microwave hydrothermal method were reported by Li *et al.* [165], showed the highest response of ~4.7 towards 0.01 vol.% C_2H_5OH at 400°C. Moreover, when compared with another material which prepared by FSP (nanoparticles) and spin coating (sensors). It was found that 3 at.% Nb-loaded TiO_2 film exhibited response of ~31.7 for 0.01vol.% C_2H_5OH at 350°C [166]. Thus, the results indicate that Pt-loaded WO_3

prepared by hydrothermal gave much higher C_2H_5OH response when compared to those of other reported.

3.3.1.3 Gas sensing of Pt-loaded WO_3 nanoparticles (H0-H1) synthesized by hydrothermal towards carbon monoxide (CO) gas

Figure 3.27 demonstrates the response ($S=R_a/R_g$) of unloaded WO_3 (S0) and 0.25–1.0 wt.% Pt-loaded WO_3 (S0.25-S1) sensors as a function of temperature when exposed to a 0.2 vol.% CO testing gas. It was found that the response of these sensors towards CO gas (with both the operating temperature and also the concentration of Pt), the sensor S1 (1.0% Pt) shows the response gradually enhanced when the working temperature was elevated up to 250°C, and then decreased with further increase in temperature. The sensor S0 (0 % Pt), S0.25 (0.25% Pt) and S0.5 (0.5% Pt) had no detectable response. Therefore, optimal operating temperature of 250°C was chosen for CO detection.

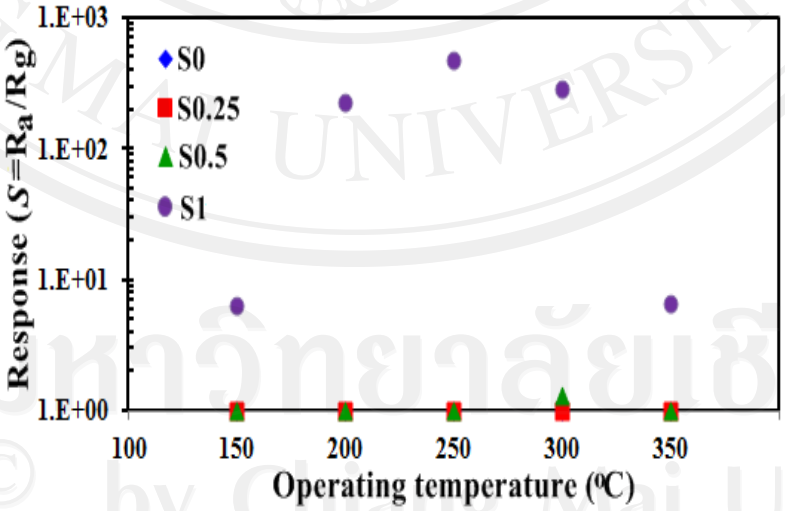

Figure 3.27 Response of the Pt-loaded WO_3 sensors towards 0.2 vol.% CO at different working temperatures.

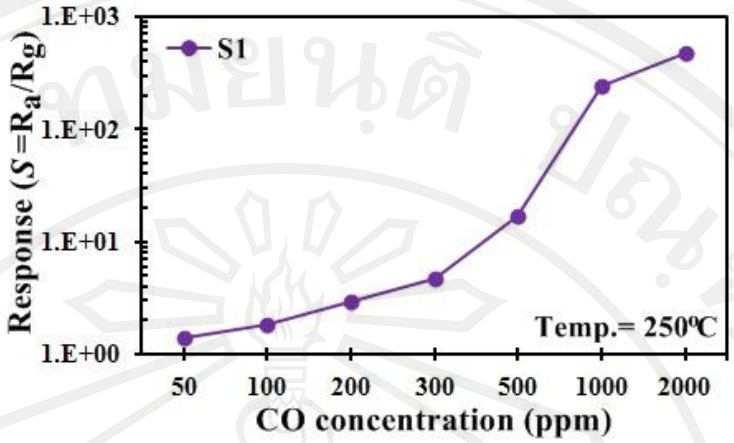

Figure 3.28 Response of the Pt-loaded WO_3 sensors towards different CO concentrations at 250°C.

The CO response dependence on gas concentration of the 1.0 wt.% Pt-loaded WO_3 sensor (S1) under the working temperature of 250°C was shown in Figure 3.28. The response increases as the CO concentration increases. The sensor has maximum gas response of 469 towards 0.2 vol.% of CO. The response time of CO was less than 3s.

According to the experimental results, it can be seen that sensor S1 showed the highest response value of ~469 at 250°C towards 0.2 vol.% CO. When compared CO response of sensor with the same material, Sberveglieri *et al.* [126] reported the unloaded WO_3 sensor was prepared by reactive sputtering. It was found that their sensor show the highest response of <0.5 towards 0.01 vol.% CO at 300−500°C. In addition, when compared with another material, Sedghi *et al.* [167] reported unloaded SnO_2 sensor which was prepared by sonochemical method. It was obvious that the sensor exhibited response of ~147 for 0.1vol.% CO at 225°C. However, 0.2 wt.% Pt/SnO_2 film showed a very low response of ~8 for 0.005 vol.% CO at

350^{o}C as reported by Mädler *et al.* [114]. Therefore, the results indicate that Pt-loaded WO_3 prepared by hydrothermal gave much higher CO response when compared to those of other reported.

3.3.1.4 Gas sensing of Pt-loaded WO_3 nanoparticles (H0-H1) synthesized by hydrothermal towards ethylene (C_2H_4) gas

The comparison between gas-sensing response ($S=R_a/R_g$) of unloaded WO_3(S0) and Pt-loaded WO_3(S0.25-S1) sensors as a function of C_2H_4 concentration between 50 and 0.1 vol.% at 350°C was shown in Figure 3.29. The sensor S1 (1.0% Pt), S0.5 (0.5% Pt) and S0.25 (0.25 % Pt) have much higher responses than sensor S0 (0% Pt). The enhanced responses should be directly related to the concentration of Pt, which could effectively catalyze the sensing reactions on the sensing layer. The unloaded WO_3, 0.25 and 0.5 wt.% Pt-loaded WO_3 sensors had the maximum gas response which were estimated to be 7.28, 35 and 349 at 0.1 vol.% of testing gas. While 1.0 wt.% Pt-loaded WO_3 sensor had the maximum gas response of 388. Moreover, the response of the unloaded WO_3 and the WO_3 nanoparticles loaded with 0.25 wt.% Pt sensing films couldn't be measured at the operating temperature beyond 200^{o}C, due to weak response signals.

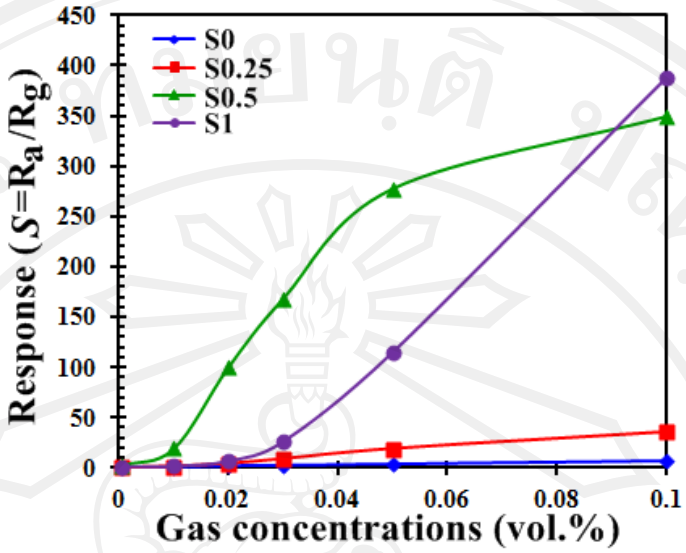

Figure 3.29 Response as function of C_2H_4 concentration for Pt-loaded WO_3 sensors at 350°C.

From the experimental results, it was found that sensor S1 showed the highest response value of ~388 at 350°C towards 0.1 vol.% C_2H_4. When compared C_2H_4 response of sensor with the same material, Pimtong-Ngam *et al.* [168] reported the unloaded WO_3 sensor which was prepared by precipitation. At the operating temperature of 300°C, the sensor showed maximum response of ~1.1 towards 6 ppm C_2H_4. In addition, when compared with another material, Jadsadapattarakul *et al.* [169] reported the unloaded SnO_2 sensor which was prepared by ultrasonic spray pyrolysis. It can be seen that sensing film showed a very low response of ~1.04 for 8 ppm C_2H_4 at 350°C. Moreover, the unloaded SnO_2 sensor which prepared by RF magnetron sputtering was reported by Ahn *et al.* [170]. The sensor exhibited response of 10.43±0.61 for 0.01 vol.% C_2H_4 at 300°C. Thus, the results indicate that Pt-loaded WO_3 prepared by hydrothermal demonstrated much higher C_2H_4 response in comparison to those of other reported.

3.3.2 Atmospheric pollution gas

3.3.2.1 Gas sensing of Pt-loaded WO_3 nanoparticles (H0-H1) synthesized by hydrothermal towards nitrogen dioxide (NO_2) gas

The response ($S=R_a/R_g$) of the unloaded WO_3 (S0) and Pt-loaded WO_3 (S0.25-S1) sensors upon exposure to 50 ppm NO_2 as a function of operating temperature is shown in Figure 3.30. It is clear that unloaded WO_3, 0.25, 0.5 and 1.0 wt.% Pt-loaded WO_3 sensors have the maximum gas response and were estimated to be 15.38, 8.21, 3.71 and 2.24 at 250°C. Therefore, the operating temperature of NO_2 gas response was obtained 250°C. The response at lower temperature (<200°C) was not satisfied, because the response decreases as the temperature increases above 250°C. At high temperature oxygen ions should preferentially occupies adsorption sites and the adsorption of NO_2 gas was suppressed.

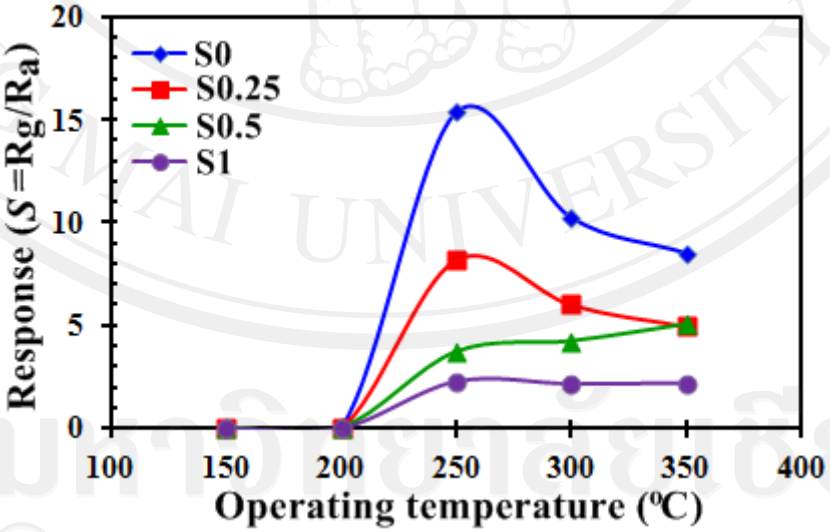

Figure 3.30 Gas sensing response of Pt-loaded WO_3 (S0-S1) sensors to 50 ppm NO_2 as a function of operating temperatures.

Figure 3.31 shows the change in resistance of the sensing films under exposure to NO_2 at various concentrations. The measurement was carried out at 250°C. The sensing films showed increasing in resistance upon exposure to NO_2, which is a unique characteristic to an n-type semiconductor. The sensing films were found to be response in the concentration range of 1−50 ppm and sensing responses were found to change upward rapidly with increase in NO_2 concentration as shown in Figure 3.32. It can be seen that the unloaded WO_3 sensor (S0) shows higher response which more than Pt-loaded WO_3 sensors. From these results, Pt catalyze is not able to increase the response but reduce responses time instead on the sensing films.

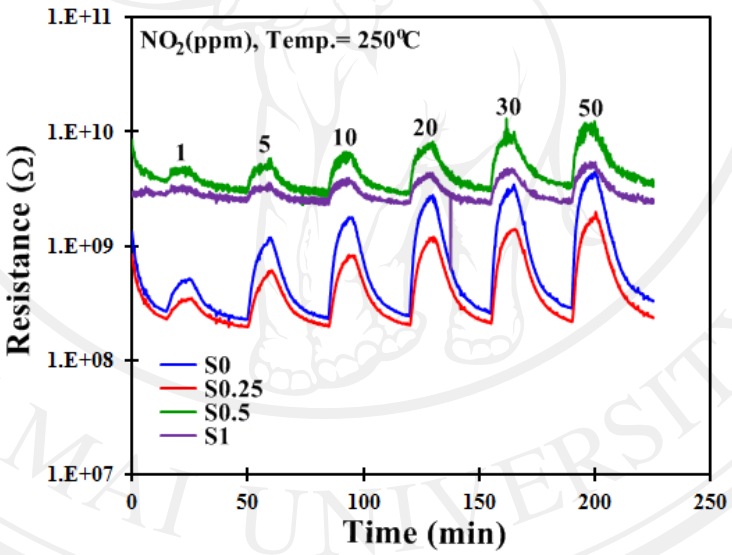

Figure 3.31 Change in resistance of Pt-loaded WO_3 (S0-S1) sensors upon exposure to NO_2 in forward cycle at 250°C.

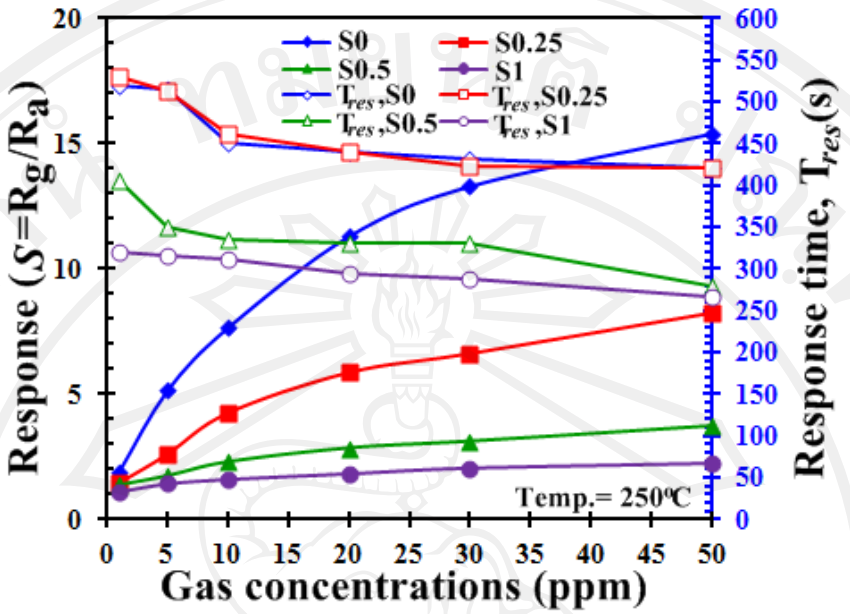

Figure 3.32 Response and corresponding response time of Pt-loaded WO_3 sensors as a function of NO_2 at 250°C.

According to the results, it was found that sensor S0 showed the highest response value of ~15.38 at 250°C towards 50 ppm NO_2. Comparing with the same material, Liu *et al.* [142] reported that the highest sensing behaviors of unloaded WO_3 to 10 ppm NO_2 was about 58 at 150°C. In addition, Liu *et al.* [144] reported unloaded WO_3 film prepared by hydrothermal, and the sensing test at 350°C with NO_2 at 20 ppm. And the sensor showed the highest response of 525. Moreover, when compared with another material, Liewhiran *et al.* [171] reported the unloaded SnO_2 nanopowders and sensor which was prepared by FSP and then spin coating to the substrate. It was obvious that thick film exhibited response of ~1640 for 20 ppm NO_2 at 200°C. Thus, the results indicate that unloaded WO_3 prepared by hydrothermal exhibited much lower NO_2 response when compared to those of other findings.

3.3.3 Selective gas sensors based on Pt-loaded WO_3 nanoparticles synthesize by the hydrothermal method

In order to determine the optimum operating temperatures, the response of the unloaded WO_3 film was measured towards 0.005 vol.% concentration of CO, C_2H_4, C_2H_5OH and NO_2 as a function of operating temperature in the ranges from 200°C to 350°C as shown in Figure 3.33. For CO and C_2H_4, the responses are very low for all temperatures. The sensor had suitable response to C_2H_5OH at high temperature (350°C) which was 3.37. However, the response of the sensor towards NO_2 was higher than to other gases, indicating that the unloaded WO_3 sensor had a high selectivity to NO_2 among the examined gases. From this figure it was obvious that the response to NO_2 increased with temperature, up to 250°C, and then gradually declined. The maximum response towards NO_2 was 15.38 at 250°C.

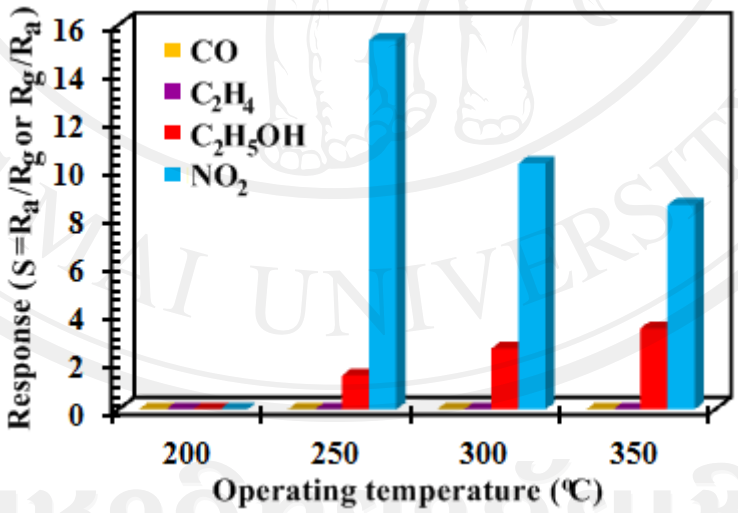

Figure 3.33 Response *versus* variation of operating of CO, C_2H_4, C_2H_5OH and NO_2 (at 0.005 vol.% concentration) for the unloaded WO_3 sensor.

To demonstrate the selectivity of Pt-loaded WO_3 sensors, the sensing responses (at operating temperature of 250°C) to various gases, namely H_2, C_2H_4, C_2H_5OH, and CO of were measured and then plotted as shown in Figure 3.34. It can be seen that sensor S1 shows much weaker responses to C_2H_5OH, CO and C_2H_4 than H_2. The response values of sensor S1 towards H_2, C_2H_5OH, CO and C_2H_4 are 2.13 x 10^3, 580, 240 and 4.86, respectively at 0.1 vol.% concentration and 250°C operating temperature. Thus, the sensor has the H_2 selectivity relative to C_2H_5OH, CO and C_2H_4 of 3.7, 8.9 and 438.3, respectively. Therefore, Pt can improve the H_2 sensing selectivity against C_2H_5OH, CO and C_2H_4.

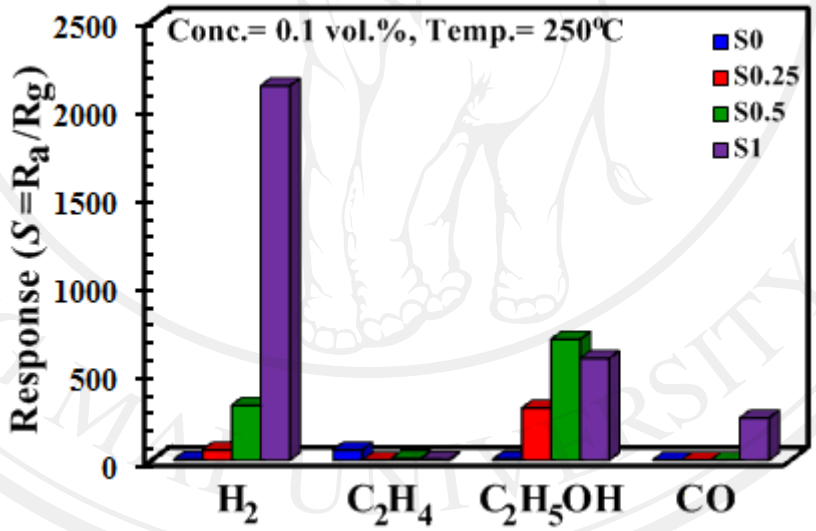

Figure 3.34 The selectivity histograms of unloaded WO_3 (S0) and 0.25–1.0 wt.% Pt-loaded WO_3 sensors (S0.25-S1) for flammable and explosive gases at concentration of 0.1 vol.% and operating temperature of 250°C.

3.4 Summary of characteristics of unloaded WO_3 and Pt-loaded WO_3 nanoparticles synthesized by FSP and the hydrothermal method.

Tables 3.2 and 3.3 show the summary of characteristics of unloaded WO_3 and Pt-loaded WO_3 nanoparticles synthesized by FSP and the hydrothermal method.

Table 3.2 Summary of characteristics of unloaded WO_3 and Pt-loaded WO_3 nanoparticles synthesized by FSP.

Material characterization methods	**Unloaded WO_3 and Pt-loaded WO_3 nanoparticles**
XRD	Monoclinic structure (JCPDS No.83−0950**)**
BET	Size : 9−10 nm
SEM	Size : 10−20 nm (nanoparticles)
TEM	Size : 5−20 nm

Table 3.3 Summary of characteristics of unloaded WO_3 and Pt-loaded WO_3 nanoparticles synthesized by the hydrothermal method.

Material characterization methods	**Unloaded WO_3 and Pt-loaded WO_3 nanoparticles**
XRD	Monoclinic structure (JCPDS No.04–006–7123)
BET	Size : 50−80 nm
SEM	Size : 40−500 nm in width and 20−40 nm in thickness (nanoplates)
TEM	Size : 80±10 nm in length and 50±5 nm in thickness

Tables 3.4 and 3.5 show the summary of gas sensing performances of unloaded WO_3 sensor synthesized by FSP and the hydrothermal method.

Table 3.4 Summary of gas sensing performances of unloaded WO_3 sensor synthesized by FSP.

Methods	**Materials**	**Gas concentration**	**Temp.**	**Response ($S=R_a/R_g$ or R_g/R_a)**
FSP	Unloaded WO_3	H_2 (0.01−1 vol.%)		No response
FSP	Unloaded WO_3	C_2H_5OH (0.005−0.1 vol.%)	200°C	~1.74 to 0.01 vol.% ~2.25 to 0.02 vol.% ~2.62 to 0.03 vol.% ~3.28 to 0.05 vol.% ~4.48 to 0.1 vol.%
FSP	Unloaded WO_3	CO (0.005−0.2 vol.%)		No response
FSP	Unloaded WO_3	C_2H_4 (0.005−0.1 vol.%)	150°C	~1.08 to 0.05 vol.% ~1.12 to 0.1 vol.%
FSP	Unloaded WO_3	NO_2 (1−50 ppm)	150°C	~3.68 to 1 ppm ~107 to 5 ppm ~247 to 10 ppm ~326 to 20 ppm ~325 to 30 ppm ~184 to 50 ppm

Table 3.5 Summary of gas sensing performances of unloaded WO_3 sensor synthesized by the hydrothermal method.

Methods	**Materials**	**Gas concentration**	**Temp.**	**Response ($S=R_a/R_g$ or R_g/R_a)**
Hydrothermal	Unloaded WO_3	H_2 (0.01−1 vol.%)	250°C	~1.6 to 0.05 vol.% ~2.86 to 0.1 vol.% ~20.2 to 0.3 vol.% ~85 to 0.5 vol.% ~102.44 to 1 vol.%
Hydrothermal	Unloaded WO_3	C_2H_5OH (0.005−0.1 vol.%)	350°C	~3.38 to 0.005 vol.% ~3.86 to 0.01 vol.% ~3.9 to 0.02 vol.% ~4.27 to 0.03 vol.% ~4.32 to 0.05 vol.% ~4.53 to 0.1 vol.%
Hydrothermal	Unloaded WO_3	CO (0.005−0.2 vol.%)		No response
Hydrothermal	Unloaded WO_3	C_2H_4 (0.005−0.1 vol.%)	350°C	~1.5 to 0.02 vol.% ~2.05 to 0.03 vol.% ~3.6 to 0.05 vol.% ~7.28 to 0.1 vol.%
Hydrothermal	Unloaded WO_3	NO_2 (1−50 ppm)	250°C	~1.9 to 1 ppm ~5.14 to 5 ppm ~7.64 to 10 ppm ~11.28 to 20 ppm ~13.28 to 30 ppm ~15.38 to 50 ppm

Tables 3.6 and 3.7 show the summary of gas sensing performances of 0.25−1.0 wt.% Pt-loaded WO_3 sensors synthesized by FSP and the hydrothermal method.

Table 3.6 Summary of gas sensing performances of 0.25−1.0 wt.% Pt-loaded WO_3 sensors synthesized by FSP.

Methods	**Materials**	**Gas concentration & Temp.**	**Response ($S=R_a/R_g$ or R_g/R_a)**
FSP	0.25wt.% Pt-loaded WO_3	H_2 (0.01−1 vol.%) Temp.=150°C	~4.73 to 0.01 vol.% ~13.54 to 0.05 vol.% ~14.8 to 0.1 vol.% ~14.44 to 0.3 vol.% ~11.6 to 0.5 vol.% ~24.3 to 1 vol.%
FSP	0.25wt.% Pt-loaded WO_3	C_2H_5OH (0.005−0.1 vol.%) Temp.=200°C	~2.7 to 0.01 vol.% ~4.26 to 0.02 vol.% ~8.88 to 0.03 vol.% ~26.5 to 0.05 vol.% ~75.1 to 0.1 vol.%
FSP	0.25wt.% Pt-loaded WO_3	CO (0.005−0.2 vol.%) Temp.=200°C	No response
FSP	0.25wt.% Pt-loaded WO_3	C_2H_4 (0.005−0.1 vol.%) Temp.=150°C	~1.09 to 0.005 vol.% ~1.1 to 0.01 vol.% ~1.15 to 0.02 vol.% ~1.23 to 0.03 vol.% ~1.28 to 0.05 vol.% ~1.74 to 0.1 vol.%
FSP	0.25wt.% Pt-loaded WO_3	NO_2 (1−50 ppm) Temp.=150°C	~4.58 to 1 ppm ~262 to 5 ppm ~637 to 10 ppm ~954 to 20 ppm ~831 to 30 ppm ~442 to 50 ppm

Table 3.6 (Cont.) Summary of gas sensing performances of 0.25−1.0 wt.% Pt-loaded WO_3 sensors synthesized by FSP.

Methods	**Materials**	**Gas concentration & Temp.**	**Response ($S=R_a/R_g$ or R_g/R_a)**
FSP	0.5 wt.% Pt-loaded WO_3	H_2 (0.01−1 vol.%) Temp.=150°C	~29.7 to 0.01 vol.% ~202 to 0.05 vol.% ~723.6 to 0.1 vol.% ~4438 to 0.3 vol.% ~7181 to 0.5 vol.% ~12688 to 1 vol.%
FSP	0.5 wt.% Pt-loaded WO_3	C_2H_5OH (0.005−0.1 vol.%) Temp.=200°C	~3.76 to 0.005 vol.% ~5.4 to 0.01 vol.% ~26 to 0.02 vol.% ~73.4 to 0.03 vol.% ~256.5 to 0.05 vol.% ~1200 to 0.1 vol.%
FSP	0.5 wt.% Pt-loaded WO_3	CO (0.005−0.2 vol.%) Temp.=200°C	~3.05 to 0.005 vol.% ~15.84 to 0.01 vol.% ~50 to 0.02 vol.% ~60 to 0.03 vol.% ~68 to 0.05 vol.% ~73.84 to 0.1 vol.%
FSP	0.5 wt.% Pt-loaded WO_3	C_2H_4 (0.005−0.1 vol.%) Temp.=150°C	~1.22 to 0.005 vol.% ~1.39 to 0.01 vol.% ~1.48 to 0.02 vol.% ~1.62 to 0.03 vol.% ~1.72 to 0.05 vol.% ~3 to 0.1 vol.%
FSP	0.5wt.% Pt-loaded WO_3	NO_2 (1−50 ppm) Temp.=150°C	~2.66 to 1 ppm ~32.57 to 5 ppm ~80.78 to 10 ppm ~124 to 20 ppm ~186 to 30 ppm ~198.55 to 50 ppm

Table 3.6 (Cont.) Summary of gas sensing performances of 0.25−1.0 wt.% Pt-loaded WO_3 sensors synthesized by FSP.

Methods	**Materials**	**Gas concentration & Temp.**	**Response ($S=R_a/R_g$ or R_g/R_a)**
FSP	1.0 wt.% Pt-loaded WO_3	H_2 (0.01−1 vol.%) Temp.=150°C	~153.6 to 0.01 vol.% ~1029 to 0.05 vol.% ~2586 to 0.1 vol.% ~16294 to 0.3 vol.% ~41598 to 0.5 vol.% ~133634 to 1 vol.%
FSP	1.0 wt.% Pt-loaded WO_3	C_2H_5OH (0.005−0.1 vol.%) Temp.=200°C	~1.22 to 0.005 vol.% ~1.39 to 0.01 vol.% ~1.48 to 0.02 vol.% ~128.5 to 0.03 vol.% ~473.5 to 0.05 vol.% ~2388 to 0.1 vol.%
FSP	1.0 wt.% Pt-loaded WO_3	CO (0.005−0.2 vol.%) Temp.=200°C	~3.82 to 0.005 vol.% ~15.28 to 0.01 vol.% ~407 to 0.02 vol.% ~800 to 0.03 vol.% ~1158 to 0.05 vol.% ~1065 to 0.1 vol.%
FSP	1.0 wt.% Pt-loaded WO_3	C_2H_4 (0.005−0.1 vol.%) Temp.=150°C	~1.35 to 0.005 vol.% ~1.84 to 0.01 vol.% ~2.45 to 0.02 vol.% ~3.79 to 0.03 vol.% ~6.7 to 0.05 vol.% ~9.9 to 0.1 vol.%
FSP	1.0 wt.% Pt-loaded WO_3	NO_2 (1−50 ppm)	~5.38 to 1 ppm ~23.34 to 5 ppm ~24.55 to 10 ppm ~ 27.46 to 20 ppm ~40.5 to 30 ppm ~58.46 to 50 ppm

Table 3.7 Summary of gas sensing performances of 0.25−1.0 wt.% Pt-loaded WO_3 sensors synthesized by the hydrothermal method.

Methods	**Materials**	**Gas concentration &Temp.**	**Response ($S=R_a/R_g$ or R_g/R_a)**
Hydrothermal	0.25 wt.% Pt-loaded WO_3	H_2 (0.01−1 vol.%) Temp.=250°C	~7.88 to 0.01 vol.% ~27.84 to 0.05 vol.% ~57.93 to 0.1 vol.% ~219.18 to 0.3 vol.% ~427 to 0.5 vol.% ~1385.36 to 1 vol.%
Hydrothermal	0.25 wt.% Pt-loaded WO_3	C_2H_5OH (0.005−0.1 vol.%) Temp.=350°C	~15 to 0.005 vol.% ~32.74 to 0.01 vol.% ~65 to 0.02 vol.% ~82 to 0.03 vol.% ~158.5 to 0.05 vol.% ~381.74 to 0.1 vol.%
Hydrothermal	0.25 wt.% Pt-loaded WO_3	CO (0.005−0.2 vol.%) Temp.=250°C	No response
Hydrothermal	0.25 wt.%Pt-loaded WO_3	C_2H_4 (0.005−0.1 vol.%) Temp.=350°C	~1.3 to 0.01 vol.% ~4 to 0.02 vol.% ~8.7 to 0.03 vol.% ~18.7 to 0.05 vol.% ~35.12 to 0.1 vol.%
Hydrothermal	0.25 wt.%Pt-loaded WO_3	NO_2 (1−50 ppm) Temp.=250°C	~1.46 to 1 ppm ~2.61 to 5 ppm ~4.24 to 10 ppm ~5.85 to 20 ppm ~6.6 to 30 ppm ~8.2 to 50 ppm

Table 3.7 (Cont.) Summary of gas sensing performances of 0.25−1.0 wt.% Pt-loaded WO_3 sensors synthesized by the hydrothermal method.

Methods	**Materials**	**Gas concentration &Temp.**	**Response ($S=R_a/R_g$ or R_g/R_a)**
Hydrothermal	0.5 wt.% Pt-loaded WO_3	H_2 (0.01−1 vol.%) Temp.=250°C	~15 to 0.01 vol.% ~92.43 to 0.05 vol.% ~312.4 to 0.1 vol.% ~2403 to 0.3 vol.% ~6990 to 0.5 vol.% ~13073 to 1 vol.%
Hydrothermal	0.5 wt.% Pt-loaded WO_3	C_2H_5OH (0.005−0.1 vol.%) Temp.=350°C	~6.46 to 0.005 vol.% ~18.6 to 0.01 vol.% ~45.6 to 0.02 vol.% ~78.5 to 0.03 vol.% ~168 to 0.05 vol.% ~674 to 0.1 vol.%
Hydrothermal	0.5 wt.% Pt-loaded WO_3	CO (0.005−0.2 vol.%) Temp.=250°C	No response
Hydrothermal	0.5 wt.%Pt-loaded WO_3	C_2H_4 (0.005−0.1 vol.%) Temp.=350°C	~2.9 to 0.005 vol.% ~19.24 to 0.01 vol.% ~100 to 0.02 vol.% ~168 to 0.03 vol.% ~277.32 to 0.05 vol.% ~349 to 0.1 vol.%
Hydrothermal	0.5 wt.% Pt-loaded WO_3	NO_2 (1−50 ppm) Temp.=250°C	~1.35 to 1 ppm ~1.72 to 5 ppm ~2.28 to 10 ppm ~2.83 to 20 ppm ~3.1 to 30 ppm ~3.7 to 50 ppm

Table 3.7 (Cont.) Summary of gas sensing performances of 0.25−1.0 wt.% Pt-loaded WO_3 sensors synthesized by the hydrothermal method.

Methods	**Materials**	**Gas concentration &Temp.**	**Response ($S=R_a/R_g$ or R_g/R_a)**
Hydrothermal	1.0 wt.% Pt-loaded WO_3	H_2 (0.01−1 vol.%) Temp.=250°C	~28.28 to 0.01 vol.% ~581.47 to 0.05 vol.% ~2130.57 to 0.1 vol.% ~8922.35 to 0.3 vol.% ~11963.9 to 0.5 vol.% ~21623 to 1 vol.%
Hydrothermal	1.0 wt.% Pt-loaded WO_3	C_2H_5OH (0.005−0.1 vol.%) Temp.=350°C	~5.57 to 0.005 vol.% ~12.28 to 0.01 vol.% ~31.56 to 0.02 vol.% ~69.87 to 0.03 vol.% ~318.74 to 0.05 vol.% ~1406 to 0.1 vol.%
Hydrothermal	1.0 wt.% Pt-loaded WO_3	CO (0.005−0.2 vol.%) Temp.=250°C	~1.4 to 0.005 vol.% ~1.86 to 0.01 vol.% ~2.95 to 0.02 vol.% ~4.74 to 0.03 vol.% ~17 to 0.05 vol.% ~240 to 0.1 vol.% ~469 to 0.2 vol.%
Hydrothermal	1.0 wt.% Pt-loaded WO_3	C_2H_4 (0.005−0.1 vol.%) Temp.=350°C	~1.1 to 0.005 vol.% ~1.5 to 0.01 vol.% ~6.76 to 0.02 vol.% ~26 to 0.03 vol.% ~115 to 0.05 vol.% ~388 to 0.1 vol.%
Hydrothermal	1.0 wt.% Pt-loaded WO_3	NO_2 (1−50 ppm) Temp.=250°C	~1.1 to 1 ppm ~1.43 to 5 ppm ~1.6 to 10 ppm ~1.82 to 20 ppm ~2.05 to 30 ppm ~2.24 to 50 ppm